JRC Scientific and Technical Reports

# Equivalent period and damping for EC8 spectral response of SDOF ring-spring hysteretic models

**Raul ZAHARIA and Fabio TAUCER**

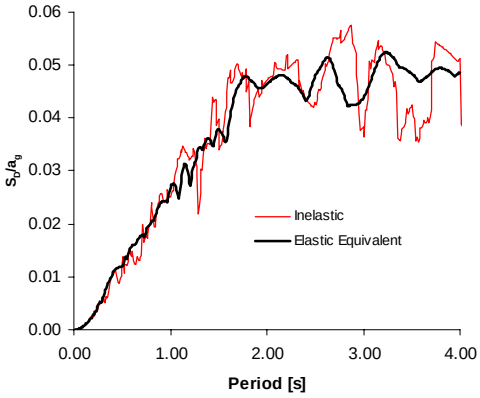


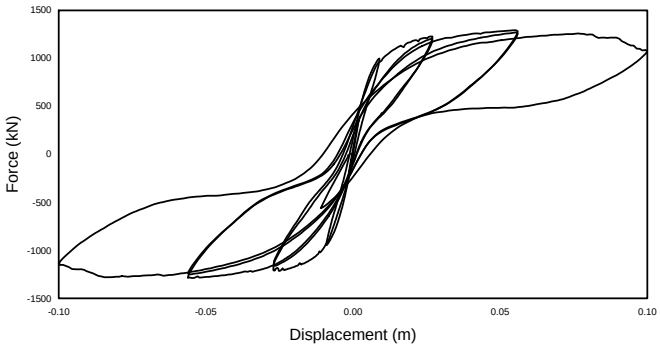


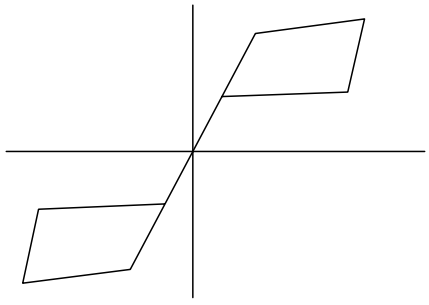

EUR 23365 EN - 2008

JRC EUROPEAN COMMISSION

ipsc Institute for the Protection and Security of the Citizen

The Institute for the Protection and Security of the Citizen provides research-based, systems-oriented support to EU policies so as to protect the citizen against economic and technological risk. The Institute maintains and develops its expertise and networks in information, communication, space and engineering technologies in support of its mission. The strong cross-fertilisation between its nuclear and non-nuclear activities strengthens the expertise it can bring to the benefit of customers in both domains.

European Commission
Joint Research Centre
Institute for the Protection and Security of the Citizen

**Contact information**
Address: Fabio Taucer TP 480, JRC Via E. Fermi 2749, I-21027 (VA)
E-mail: fabio.taucer@jrc.it
Tel.: +39 0332 78.5886
Fax: +39 0332 89.9049

http://ipsc.jrc.ec.europa.eu/
http://www.jrc.ec.europa.eu/



JRC 45403

EUR 23365 EN
ISSN 1018-5593

Luxembourg: Office for Official Publications of the European Communities



*Printed in Italy*

# Abstract

The following report presents a procedure to determine the equivalent properties of a viscoelastic linear model capable of approximating the maximum earthquake response of a SDOF ring-spring hysteretic system, representative of the cyclic behaviour of lightly reinforced concrete bridge piers, for a series of synthetic ground motions compatible with Type 1 and Type 2 Eurocode 8 spectra. The results show that the displacements obtained from the equivalent model approximate well the results obtained from the nonlinear model, and that the coefficients of the expressions for determining the equivalent properties depend on the family of earthquakes considered in the analysis. Expressions for determining the secant stiffness and equivalent damping corresponding to the energy dissipated by harmonic cycles at maximum displacement are derived for the ring-spring model and a relationship for computing a reduction factor of the maximum ductility is proposed such that the equivalent properties computed from these expressions approximate those obtained from the error minimization process. Recommendations to improve the error minimization process and the derivation of equivalent properties are proposed at the end of the report.

# Acknowledgements

The work of the present report was prepared within the framework of the Exploratory Research granted by the Institute for the Security of the Citizen during the year 2004, and as part of the institutional action SAFECONSTRUCTION of the ELSA Unit, Joint Research Centre.

Raul Zaharia was a JRC grant holder (Category 30, Post-Doctoral) for the time period from 16.02.2003 to 15.02.2005, funded through Contract No. 20135-2002-11 P1B30 ISP IT; he now holds a position of associate professor at the Universitatea “POLITEHNICA” Timisoara.

The contribution of Pierre Pegon (ELSA Unit, JRC) in coding the ring-spring hysteretic model into the finite element model CAST3M software is acknowledged.

# Table of Contents

# 1 Introduction

The development and innovation of construction codes and norms is the result of a constant effort that involves the international scientific community as a whole. As more knowledge is gathered from the collection of experimental and numerical data generated from research institutions throughout the world, our capabilities for understanding the problems and improving the analysis and design of structures have improved significantly. However, these advances have also generated an increase in the complexity of the proposed design methodologies that in most cases cannot be implemented by practicing engineers.

In addition, the consequences of destructive earthquakes have called the need to consider in the design of structures not only life-safety issues, but also economic and functionality aspects, resulting into what is known today as Performance Based Design (PBD), which sets the performance of a given structure in terms of its function, the frequency of the earthquake event and the accepted level of damage. For example, a given structure may be designed to suffer little damage under the action of frequent earthquakes (low magnitude), while for more infrequent ones (large magnitude) the same structure is required to protect the life of its occupants while accepting large levels of damage. Similarly, under a large magnitude earthquake, hospitals may be required to respond with low levels of damage so as to remain functional to attend the injured, while for residential buildings large levels of damage are usually accepted.

The concept of PBD calls for determining the response of a structure with analytical procedures beyond the scope of current construction norms. Numerical analytical tools by means of nonlinear dynamic Finite Element Analysis (FEM) have been available for many years to researchers and expert engineers, and permit to compute the structural response needed to satisfy PBD. However, these tools are not used in practice and are too time consuming to be used realistically for the design of new structures. In addition, the results of nonlinear dynamic FEM analysis depends largely on the type of earthquake excitation chosen, creating a considerable degree of uncertainty in the design.

For the reasons exposed above, researchers have proposed the use of simplified numerical tools to replace the nonlinear dynamic FEM analysis in the design phase of structures and for the preliminary assessment of existing ones. Among these, some are based on response spectrum analysis of nonlinear systems linearized to equivalent values of stiffness and damping to compute peak response. This methodology offers the advantage of using response spectra to represent the earthquake excitation: the spectral demands are smooth and are univocally defined by the design codes. The main variables controlled in PBD are no longer forces, as considered in present design codes, but displacements. This design approach, in which the displacements are used to judge the performance of the structure, is called Displacement – Based Design (DBD).

Considerable work has been carried out in the past to determine the equivalent properties of linearized nonlinear systems capable of determining earthquake peak response. Most of the research has been conducted by computing secant stiffness properties and energy dissipated at peak displacement from cyclic harmonic response on a large spectrum of nonlinear hysteric models, or by extracting the best combination of equivalent properties in terms of stiffness and damping to match in statistical terms the nonlinear response to a family of earthquake ground motions and nonlinear models. This report focuses on following the second approach for earthquake ground motions compatible with EC8 and for a particular nonlinear model for which work on equivalent properties has not been studied in depth in the past, namely, the ring-spring hysteretic model, representative of the cyclic behaviour of lightly reinforced concrete bridge piers.

The report starts by reviewing the principles of displacement-based seismic design and the various models to describe the equivalent properties of linear systems representing nonlinear response, with particular emphasis on the methodologies considering a modification of both the initial period and damping of the system, based on the use of empirical formulas to minimise the error between the response of the nonlinear and the linear equivalent models using linear and nonlinear time-history analysis.

The generation of synthetic time histories compatible with EC8 Type 1 and Type 2 response spectrum for various levels of earthquake magnitude and soil types is described in detail. The procedure adopted for computing the stiffness (period) and damping properties of the equivalent model is described step by step, highlighting the differences with respect to the methodologies adopted by previous researchers.

Expressions for period shift and equivalent damping in terms off ductility are derived for two types of hysteretic models: a bilinear kinematic model and four ring-spring models, considering Type 1 and Type 2 response spectra, for a total of 10 expressions. The results of a kinematic model are used as benchmark for comparing the results with those obtained from the ring-spring model. The accuracy of the proposed expressions is evaluated with respect to the exact response, in terms of the average and standard deviation for the range of ductilities considered in the analysis.

The results from the analysis are discussed, with concluding remarks and recommendations.

# 2 Principles of Displacement-Based Seismic Design

Traditionally, seismic design approaches are force-based, and have remained up until recently, the basis of most current codes (FIB, 2003). Although the ductility developed by members is the fundamental parameter to determine the reduction factors for the computation of seismic lateral forces - and this approach implies assuming a displacement capacity - the design is still carried out in terms of a required strength. In the last decade, several researchers have proposed displacement-based approaches for earthquake engineering analysis and design, which deal directly with displacement demands. The aim is to provide improved reliability in the design process by directly relating the computed response with the expected structural performance.

A recent state-of-the-art report, prepared by Task Group 7.2 “Displacement-based design and assessment” of the International Federation for Structural Concrete (FIB, 2003), summarises the displacement-based approaches proposed in literature; for the purposes of the present research, only the substitute structure method proposed by Shibata and Sozen (1976) is described. In this approach, the real non-linear MDOF structure is replaced by an elastic SDOF structure, having an equivalent stiffness (or period) and equivalent viscous damping ratio. This equivalent elastic structure is supposed to have the same peak response as the real non-linear structure under earthquake excitation. The substitute structure being elastic, its response to a particular earthquake can be determined from elastic response spectra calculated for a given equivalent damping ratio as a function of the equivalent period.

For example, consider a structure having an initial stiffness $K_{cr}$, a post-yielding stiffness $K_h$ and a yield displacement $\Delta_y$, as shown in Fig. 2-1a. Assuming an allowable ultimate displacement $\Delta_u$, the initial ductility ratio $\mu = \Delta_u/\Delta_y$ is computed. The equivalent (effective) viscous damping $\xi_{eff}$ is then computed as a function of the ductility ratio considering an adequate hysteretic model.

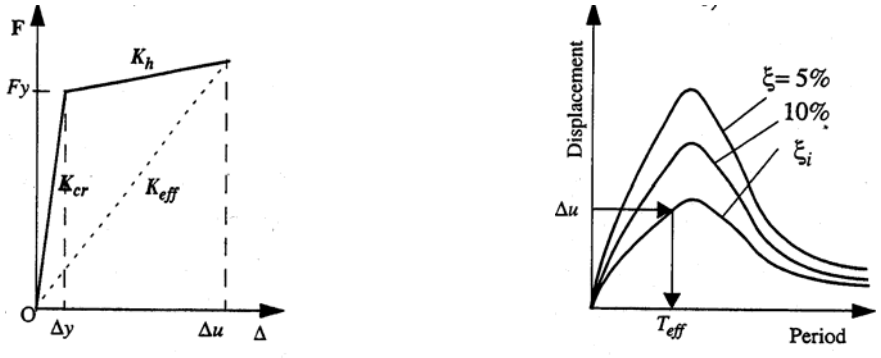


a) Equivalent stiffness

b) Displacement response spectrum

Fig. 2-1 Displacement-based design

From the elastic displacement response spectra derived for the equivalent viscous damping $\xi_{eff}$, the equivalent (effective) period of the linear system $T_{eff}$ is computed as a function of target displacement $\Delta_u$, as indicated in Fig. 2-1b. The structure design forces are computed from the equivalent stiffness $K_{eff}$, which is derived from $T_{eff}$. The yield displacement $\Delta_y$ is then revised and subsequent iterations occur until convergence is reached.

One of the main problems in applying this method to SDOF systems is the calculation of the equivalent viscous damping ratio and equivalent stiffness (or period) of the elastic equivalent system to predict the inelastic response of nonlinear systems to earthquake excitation. Several equivalent damping models exist in the literature and are reviewed in the following chapter.

# 3 Review of Equivalent Models

The first author to introduce the equivalent viscous damping concept was Jacobsen (1930). The approach was initially used to approximate the steady-state response of a SDOF system having the following differential equation:

$$m\ddot{x} + F(\dot{x}) + kx = F_0 \sin \omega t \tag{3.1}$$

with the steady-state response of an equivalent linear oscillator with a nonlinear damping function and the following equation of motion:

$$m\ddot{x} + c(x_0)\dot{x} + kx = F_0 \sin \omega t \tag{3.2}$$

in which:

- $m$ mass of the oscillator
- $x$ displacement of the oscillator
- $\dot{x}$ velocity of the oscillator
- $\ddot{x}$ acceleration of the oscillator
- $k$ stiffness of the oscillator
- $F_0$ amplitude of the exciting force
- $\omega$ circular frequency,
- $F(x)$ damping function, depending on the instantaneous value of the oscillator velocity,
- $x_0$ steady-state response amplitude
- $c(x_0)$ equivalent damping coefficient

The equivalent damping coefficient is determined so that the nonlinearly damped oscillator and the equivalent linear system dissipate the same amount of energy per cycle of response to the sinusoidal excitation. In this study, the stiffness of the equivalent linear oscillator was considered equal to the stiffness of the original system. This approach was proposed for a rather broad category of damping functions: for example, the damping function could be any convergent power series in velocity (Jacobsen, 1960).

The same author (Jacobsen, 1960) highlighted the problems that appear in the attempt of finding an equivalent linearization method for the case of steady-state response of yielding SDOF systems. For yielding systems, the increase in period with amplitude, in the post-elastic range, causes problems that are not present when an equivalent linear structure is used to describe the steady-state response of an elastic system as described by Equation (3.1). If both the period shift and the amplitude variations are to be modelled, the equivalent linear system should have a variable period as well as a variable damping coefficient. The damping coefficient $c$ of the equivalent oscillator should vary to account for the non-linearities of the energy dissipation of the yielding oscillator. Also, the critical damping $c_{cr} = 2(mk)^{0.5}$ should change if the stiffness (period) of the equivalent system changes due to the period shift of the yielding oscillator.

Jennings (1968) makes a review of six proposals of equivalent linearization methods, based on the Jacobsen (1930) approach, for the case of steady-state response of yielding SDOF systems. The author noted that the different methods of treating the period shift are the main causes for the different behaviour of equivalent viscous damping factors of yielding structures. It was shown that the linear equivalent models for determining the steady-state yielding response of SDOF systems are described by the general equation:

$$m(x)\ddot{x} + c(x_0)\dot{x} + k(x_0)x = F_0 \sin \omega t \tag{3.3}$$

in which $m(x_0)$, $c(x_0)$ and $k(x_0)$ are, respectively, the mass, the damping and the stiffness of the equivalent linear system, function of the steady-state response amplitude $x_0$. For most methods, the mass of the associated linear oscillator does not vary and is equal to the mass of the yielding oscillator $m$, leaving the other two parameters to be determined. The associated equivalent linear system is subjected to the same sinusoidal excitation as the yielding system.

The yielding oscillator shown in Fig. 3-1 shows the force-displacement relation of an elasto-plastic hysteretic model, for which the equivalent linear oscillator was determined using the methods reviewed by Jennings (1968). In this figure, $x_y$ is the yield displacement, $P_y$ the yielding force and $k$ is the stiffness of the original oscillator.

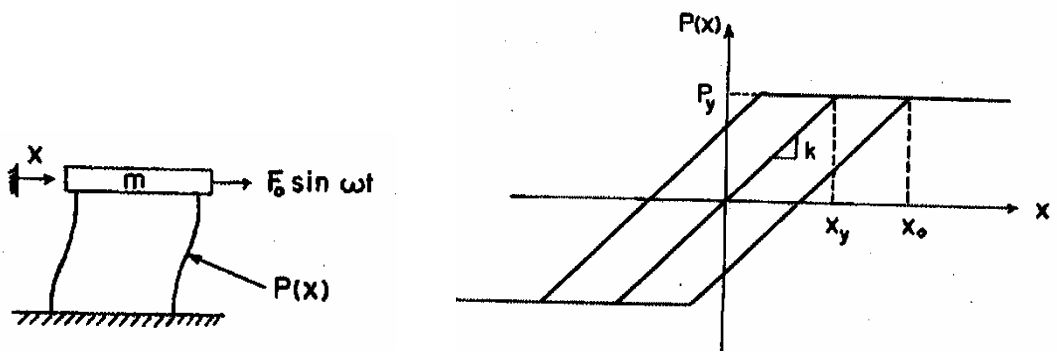


a) SDOF Yielding oscillator b) Elasto-plastic hysteretic model

Fig. 3-1 Yielding oscillator

As in Jacobsen (1930) approach, the equivalent viscous damping of the linear oscillator is obtained by equating the dissipated energy per cycle of the original oscillator ($E_p$) to that of the equivalent linear system ($E_e$). The energy dissipated per cycle of vibration by the elasto-plastic system is the area of the hysteretic loop as shown in Fig. 3-1b, and is calculated as:

$$E_p(x_0) = 4kx_y(x_0 - x_y) \tag{3.4}$$

For the associated linear oscillator of Equation (3.3), the critical damping coefficient, the damping ratio and the energy dissipated per cycle, function of the amplitude of the steady-state response (Jennings, 1968), are:

$$c_{cr}(x_0) = 2\sqrt{m(x_0)k(x_0)} \tag{3.5}$$

$$\xi(x_0) = \frac{c(x_0)}{c_{cr}(x_0)} \tag{3.6}$$

$$E_e(x_0) = 2\pi\xi(x_0)k(x_0)x_0^2 \tag{3.7}$$

For all the six methods reviewed by Jennings (1968), Equations (3.4) through (3.7) remain the same. The difference between these methods results from the way the three parameters of the linear equivalent system (mass, damping and stiffness) are varied. From these methods, only the Geometric Stiffness Method proposed by Rosenblueth and Herrera (1964) is discussed in the following. This method was the first one to propose the secant stiffness at maximum amplitude as the basis for selecting the period shift, in which the stiffness of the associated linear system is determined from the geometry of an elasto-plastic force-displacement relation as presented in Fig. 3-1b, equal to the slope of the line joining the ends

of the hysteretic loop. According to the notation of Fig. 3-1b, the stiffness of the equivalent linear system is expressed as:

$$k(x_0) = k\frac{x_y}{x_0} \tag{3.8}$$

By equating the dissipated energy per cycle of the equivalent linear system from Equation (3.7) to the dissipated energy per cycle of the real oscillator from Equation (3.4), and considering the expression of equivalent stiffness from Equation (3.8), it is possible to compute the equivalent damping ratio:

$$\xi(x_0) = \frac{2}{\pi}\left(1-\frac{x_y}{x_0}\right) \tag{3.9}$$

In a more general formulation, considering the definition of ductility ratio $\mu$, and adding the viscous damping ratio $\xi_0$ of the yielding system, the above formula may be expressed as follows:

$$\xi_{eq} = \xi_0 + \frac{2}{\pi}\left(1-\frac{1}{\mu}\right) \tag{3.10}$$

Together with the equivalent damping ratio, the second parameter used in equivalent linearization methods using secant stiffness at maximum amplitude is the equivalent period $T_{eq}$. Considering the secant stiffness definition from Equation (3.8), the equivalent period is determined as a function of the initial period of the yielding system $T_0$ and of the ductility ratio:

$$T_{eq} = T_0\sqrt{\mu} \tag{3.11}$$

Equations (3.10) and (3.11) are further generalised for the case of a bilinear hysteretic model, considering a post yield-to-initial stiffness ratio $r$. Thus, the complete expressions proposed by Rosenblueth and Herrera (1964) for equivalent damping ratio and equivalent period are:

$$\xi_{eq} = \xi_0 + \frac{2}{\pi}\left[\frac{(1-r)(\mu-1)}{\mu - r\mu + r\mu^2}\right] \tag{3.12}$$

$$T_{eq} = T_0\sqrt{\frac{\mu}{1-r+r\mu}} \tag{3.13}$$

In a later study, Gulkan and Sozen (1974) showed that ductility by itself is not sufficient to interpret the behaviour of reinforced concrete structures. Two systems having the same ductility, defined with respect to a load deformation curve obtained from a load monotonically increased to failure, may not have the same response to a cyclic excitation if the hysteretic properties of the two systems differ. Thus, for a given period shift, the hysteretic model considered also leads to changes in the equivalent damping. Until Jennings (1968) review, all the equivalent linearization methods considered only the bilinear model.

Moreover, all these methods were based on harmonic loadings. Under non-harmonic excitation, which is the case of earthquake loading, the response of the yielding system is more complex and the cycles of deformation are in general of smaller amplitude than the cycle at peak response used to compute the equivalent damping. As a result, the equivalent damping is overestimated, leading to smaller earthquake response of the equivalent system.

Gulkan and Sozen (1974) emphasised that two basic characteristics of reinforced concrete structures play an important role in determining their response to strong ground motions: the changes in stiffness and the energy dissipation capacity, which are related to the maximum displacement. The authors proposed a new formula for the equivalent damping ratio, based

on the results from shaking table tests performed on a series of reinforced concrete frames subjected to steady-state dynamic base motions and simulated earthquake motions. From the tests it was observed a discernible evolution of the equivalent damping factor with the ductility ratio, a trend consistent with Jacobsen (1930) approach using a Takeda model with degrading-stiffness-hysteretic-response (Takeda et. al, 1970). Considering a symmetrical loop, as shown in Fig. 3-2, the degrading stiffness is defined by the slope of line BC, function of the slope corresponding to a fully cracked section, ductility ratio $\mu$, and a parameter $\alpha$ calibrated from test results. The slope AB represents the secant stiffness (effective stiffness of the linear system).

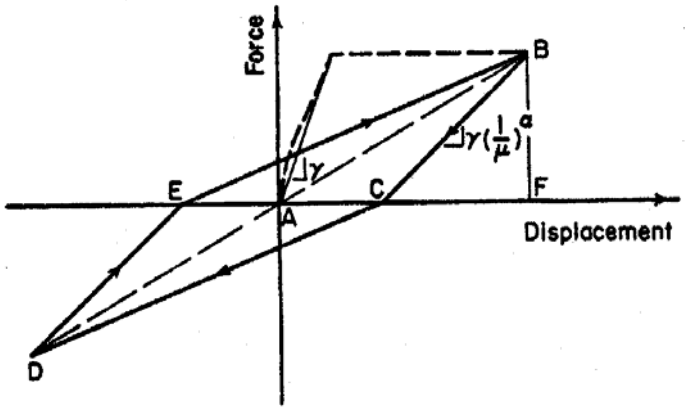


Fig. 3-2 Takeda degrading stiffness model

Considering the symmetry of the loop and according to Jacobsen (1930) approach, the equivalent damping ratio is computed by equating the area EBC (the dissipated energy of the real oscillator) to area ABF (the dissipated energy of the equivalent linear system). The following formula is obtained for the equivalent damping ratio:

$$\xi = \xi_0 + 0.2\left(1 - \frac{1}{\mu^{0.5}}\right) \tag{3.14}$$

The authors emphasize that, considering the scatter of experimental data, the value of the equivalent damping ratio computed with the above formula represents a range rather than a precise quantity. As in Rosenblueth and Herrera (1964) approach, the secant equivalent stiffness at maximum displacement is used, so that the equivalent period of the linear system is computed with Equation (3.11).

Although the study used only one earthquake motion, simulating the N21E component of the 1952 Taft record, the authors claimed that this approach is also suitable for direct use with compatible response spectra, representative of a large class of earthquake ground motions.

In a later study, Iwan and Gates (1979, 1980) used results from time-history analyses of 12 recorded earthquake ground motions, in order to calibrate empirical formulas for the equivalent damping ratio and period shift of an equivalent linear system. The time histories were scaled in acceleration to minimize the standard deviation of their displacement spectra with respect to a reference displacement spectrum in the period range 0.4 – 4.0 s. The hysteretic model used in this study for the time-history analysis was derived from a combination of linear elastic and Coulomb slip elements, which were divided in three groups: a single elastic element, an elasto-plastic group and a group capable of modelling stiffness degradation (cracking and crushing).

Six specific systems were considered, covering a wide range of hysteretic load-deformation behaviour, as show in Fig. 3-3. The post-yield stiffness was also considered, and set in all cases to 5% of the elastic stiffness.

The symbol BLH for the first model in Fig. 3-3 denotes the bilinear hysteretic model. The three number code for the other five models represent, respectively, the ratio of the strength of the

yielding component to that of the degrading component, the ratio of the generalized displacement between yielding and crushing, and the ratio of cracking to crushing strength.

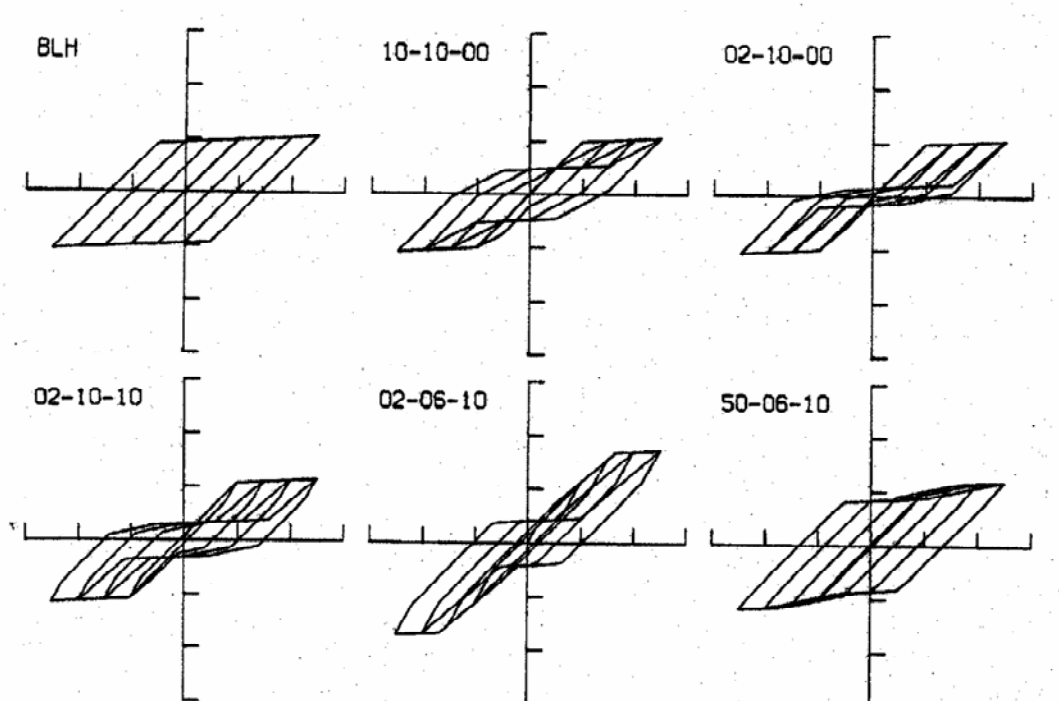


Fig. 3-3 Hysteretic models (From Iwan, 1980)

The response of each structural model to ground motion was calculated by numerical integration of the differential equation of motion with a viscous damping of 2%, while the yield level of the structural model was varied until a specified ductility ratio was obtained. In this way, the resulting maximum displacements, determined as a function of the ductility ratio, were used to construct inelastic displacement response spectra for each hysteretic system and earthquake as a function of the ductility ratio. Inelastic displacement response spectra were constructed for ductility ratios of 2, 4 and 8, considering nine spectral periods between 0.4 and 4 s.

Iwan and Gates (1979, 1980) observed that by converting spectral displacement to a normalized pseudo-velocity (PSV) spectrum, the overall shape of the inelastic spectrum for a given value of ductility ratio closely resembles that of a linear spectrum if that spectrum is shifted in period by some given factor. This indicated that it was possible to obtain the “best” fit of the inelastic response by a correct estimation of the damping and period shift of a linear system, i.e., to find the optimal equivalent linear system parameters. By representing the optimal damping ratio versus optimal period shift ratio for all the considered systems and ductilities, all the earthquake ground motions, and the optimal period shift ratio versus ductility ratio, an empirical set of formulas was determined to fit the available data. The following expressions were determined for the equivalent period and damping ratio of the linear system:

$$T_{eq} = T_0\left[1+0.121\left(\mu-1\right)^{0.939}\right] \tag{3.15}$$

$$\xi_{eq} = \xi_0 + 5.87\left(\mu-1\right)^{0.371} \tag{3.16}$$

For all systems and ductility ratios considered, these empirical formulas give an overall root-mean-square averaged spectral error of 11%.

In a more recent theoretical study, Kowalsky (1994) used the secant stiffness at maximum deformation for defining the period shift, as in Rosenblueth and Herrera (1964) and Gulkan and Sozen (1974) models, together with the Takeda hysteretic model for degrading-stiffness-

hysteretic-response (Takeda et. al, 1970). Using the Jacobsen (1930) approach, i.e., equating the energy dissipated by one cycle of the real oscillator to one cycle of sinusoidal response of the equivalent linear system (with secant stiffness defined at maximum deformation), the author showed that the equivalent damping may be obtained, with reference to Fig. 3-4, from the following equation:

$$\xi_{eq} = \frac{2}{\pi}\frac{A_1}{A_2} \tag{3.17}$$

In which $A_1$ is the area of the nonlinear hysteretic loop (arbitrary) and $A_2$ the area of the rigid-perfectly plastic loop that passes through the maximum displacement.

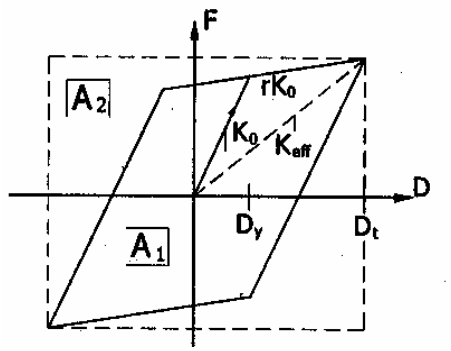


Fig. 3-4 Equivalent damping approach

The equation presented above was derived for steady state under harmonic excitation; therefore it is an approximation for earthquake excitation. Using this formula, and considering the Takeda (1970) hysteretic model for an unloading stiffness factor $\alpha$ of 0.5 (with reference to Fig. 3-2) and for a post yield to initial stiffness ratio *r*, the equivalent damping ratio is given by:

$$\xi_{eq} = \xi_0 + \frac{1}{\pi}\left(1 - \frac{1-r}{\mu^{0.5}} - r\,\mu^{0.5}\right) \tag{3.18}$$

For a post yield-to-initial stiffness ratio *r* equal to zero, the equivalent damping ratio is expressed as:

$$\xi_{eq} = \xi_0 + \frac{1}{\pi}\left(1 - \frac{1}{\mu^{0.5}}\right) \tag{3.19}$$

For a post yield yield-to-initial stiffness ratio *r*, the period shift is computed with Equation (3.13) in association with Equation (3.18), while for a post yield-to-initial stiffness equal to zero, the period shift is computed with Equation (3.11) in association with Equation (3.19).

It must be emphasised that the amount of energy absorbed in the loop of the Takeda model changes with each cycle. However, after several cycles have been carried out at the same maximum displacement, the shape of the loop stabilises, absorbing less energy than in the initial cycle corresponding to that displacement. This assumption, conservative for design purposes, was considered in determining Equation (3.18).

It may be observed that Equation (3.19) is similar to Equation (3.14), with the exception that the constant term multiplying the ductility function of the equation leads in Kowalski's method to a higher value of the equivalent damping.

Of particular interest to practicing engineers is to have information on which of the equivalent linearization methods produces better results for specific periods of vibration or at least for specific spectral regions, as well as to establish which method provides better results for the levels of inelastic behaviour expected to occur in the structure. This was the purpose of the

Miranda and Ruiz-Garcia (2002) study, in which the authors evaluated the four methods described above, i.e., Rossenblueth and Herrera (1964), Gulkan and Sozen (1974), Iwan and Gates (1979, 1980) and Kowalski (1994). A comparison between the “exact” results computed with non-linear time-history analyses and those computed with the approximate methods was made. In this evaluation, three types of hysteretic behaviour were considered: an elasto-plastic model, the modified Clough stiffness-degrading model (Clough and Johnston, 1996; Mahin and Lin, 1983) and the Takeda (1970) model. The post elastic stiffness, for all models, was set equal to zero and the damping ratio at 5%. A set of 50 periods of vibration between 0.05 and 3 s were considered, and a total of 264 earthquake acceleration time-histories recorded in the state of California (USA) for 12 different earthquakes, were used in this evaluation.

Miranda and Ruiz-García concluded that the Rosenblueth and Herrera method significantly underestimates the maximum inelastic displacement of the three types of hysteretic models considered in the study. The result is not surprising, as the normalised damping ratios of the four methods (product of the equivalent damping ratio and the ratio of the initial to equivalent stiffness) show significant higher values for the Rosenblueth and Herrera method, which is based on the elasto-plastic hysteretic model and steady-state harmonic response. The other methods were calibrated for degrading stiffness hysteretic models and have been developed specifically for seismic loading. The smallest normalised equivalent damping ratios are those corresponding to the Gulkan and Sozen method, while the corresponding values for Iwan and Gates, and Kowalsky’s methods are relatively close to each other.

For the Gulkan and Sozen, Iwan and Gates, and the Kowalski’s methods, the mean relative errors in predicting peak inelastic response increases generally with increasing ductility ratios and with decreasing periods. In general, these methods produce more accurate results in comparison with the “exact” response of the nonlinear SDOF system in the intermediate and long period range regions. In the short period spectral region, the Gulkan and Sozen and the Kowalsky’s methods tend to significantly overestimate the maximum displacements. Iwan’s method yields the best estimations of maximum displacements, noting that, for periods lower than 0.4 s, it underestimates the maximum displacement.

The conclusion of the Miranda and Ruiz-García study was that, despite having relatively small mean errors, the dispersion of the results in some cases is substantial, in particular for large levels of inelastic behaviour (ductility). Hence, when applied to individual earthquake ground motions, any of these methods could lead to significant errors in the estimation of the maximum displacement.

Dwairi and Kowalsky (2004) have also obtained the same conclusion. The authors investigated the accuracy of the equivalent viscous damping concept, as stated by Jacobsen (1930), when applied to real earthquake records. In this study, the Takeda hysteretic model (1970) and Ring-Spring hysteretic model (Hill, 1968; Blandon, 2004), shown in Fig. 3-5, were considered, and were used to compute expressions of displacement ductility and equivalent damping ratios, using the Jacobsen approach illustrated in Equation (3.17).

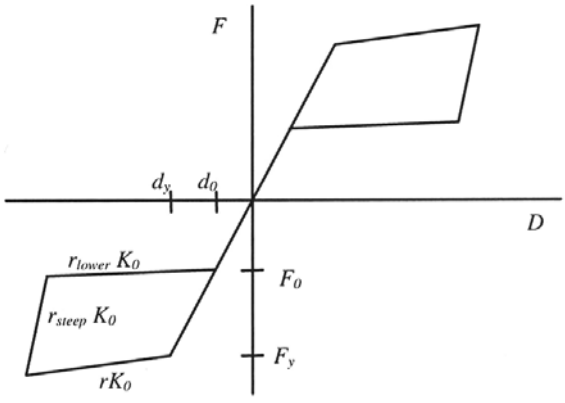


Fig. 3-5 Ring-Spring hysteretic model

In determining the expressions of equivalent damping for the Takeda model, two extreme cases were selected by changing the model parameters: the smallest and the largest possible loop. The novelty of this approach is that it considered hysteretic models with low and high energy dissipation. For the Ring-Spring model, only the largest possible loop was considered in determining the equivalent damping ratio expression.

The results from two earthquake records, with distinctly different response spectra, showed a very wide scatter for the three hysteretic models selected, both conservative and unconservative. A wide scatter was noticed in the short period region, where the oscillator vibrates about its fundamental frequency, while less scatter was noticed in the long period range, where the oscillator vibrates about its loading function frequency. By comparing the results of both records, Dwairi and Kowalsky concluded that Jacobsen's approach was not only sensitive to the earthquake characteristics, but also to the oscillator fundamental period and level of ductility. The scatter was quantified by performing a statistical analysis on a large number of results obtained from a number of simulated earthquakes. For this, 100 earthquakes were selected, with 50 oscillators with fundamental periods ranging from 0.1 to 5 s. The total number of inelastic time-history analyses conducted in this part of the study was 125 thousand; the results were plotted considering the equivalent damping and period of the oscillator, and averaged to smooth out the effect of the earthquake characteristics.

Dwairi and Kowalsky concluded that the hysteretic models with lower levels of damping (Takeda small loop) produce better results, suggesting that the Jacobsen's approach, on average, overestimates damping and consequently underestimates actual displacements. This indicates that a reduction factor could be used to improve the results. For this purpose, the authors recommended to perform a more complex study, comprising 4 hysteretic models and 280 thousand time-history analyses.

In a more recent study, Blandon and Priestley (2004, 2005) compared the equivalent viscous damping estimated by Jacobsen's approach for steady-state harmonic response with the effective damping factors obtained from an iterative procedure using time-history analyses of SDOF systems. Six hysteretic models (elasto-plastic, bilinear to model a structure incorporating an isolation device, Takeda "fat" and "thin", Ramberg Osgood and ring-spring) and six artificial records compatible with ATC32 (1996) design spectrum for soil type C were used in the analysis. The authors concluded that the Jacobsen's approach overestimates the values for equivalent viscous damping and proposed modified design equations for equivalent viscous damping:

$$\xi_{eq} = \frac{a}{\pi}\left(1-\frac{1}{\mu^{b}}\right)\left(1+\frac{1}{(T+c)^{d}}\right)\frac{1}{N} \tag{3.20}$$

in which $a$ and $d$ are coefficients determined for each hysteretic model, $\mu$ is the ductility, $T$ is the effective period and $N$ is a normalizing factor. This expression improves the formulas determined in a previous research by Priestley (2003). The procedure for determining the coefficients of the equation was based on matching the maximum displacement response for a SDOF system at a given level of ductility with the maximum displacement of an equivalent elastic system having the same period and an appropriate equivalent damping. The process considered eight periods (from 0.5 s to 4 s, with a step of 0.5 s) and five ductility levels, from 2 to 6, for the six artificial records.

In general, it may be concluded that no direct displacement-based design method, based on equivalent linearization, is able to produce precise results for any arbitrary given real earthquake record. Most of the proposed methods use a theoretical approach, assuming a steady-state sinusoidal response, and are based on the arbitrary choice of estimating the equivalent viscous damping from the area contained in a full cycle. The energy dissipation of the system is computed from the cycle corresponding to the maximum level of deformation, assumed to be symmetric and with the same shape for the entire excitation time. For earthquake loading, the use of this criterion overestimates the amount of equivalent damping, as during the time history response the cycles of deformation are in general of smaller amplitude than the cycle at peak response used to compute the equivalent damping. At the same time, the equivalent stiffness is computed as a function of the maximum level of deformation, leading for a particular earthquake, to a wide dispersion in the estimation of the

maximum displacement. Methods combining the theoretical “equivalent energy” approach with testing or numerical analysis seem to be more reliable when applied to real earthquake records.

From the methods considered in this literature review, an empirical approach similar to the one proposed by Iwan and Gates (1979, 1980) seems to be the most suitable to overcome the underlined deficiencies for estimating equivalent linear parameters to produce reliable results for earthquakes compatible with a given response spectra.

# 4 Determination of Equivalent Properties

The methodology for determining the equivalent stiffness and equivalent damping of nonlinear systems for Eurocode 8 response spectra compatible earthquakes is inspired from the empirical approach of Iwan and Gates (1979, 1980) presented in the previous section.

The methodology is as follows: for a family of earthquake records compatible with a given acceleration response spectra, and for a given structural model (hysteretic model), the inelastic displacement response is calculated by numerical integration for different ductility ratios. After determining the elastic displacement response spectrum for different values of damping and period shift, the optimal pair of these equivalent linear parameters is determined. The optimal equivalent parameters correspond to the elastic displacement spectrum that gives the lowest averaged error in comparison with the “exact” inelastic displacement spectrum. By representing the optimal period shift against ductility, and the optimal equivalent damping against the optimal period shift, empirical formulas for equivalent period and damping are obtained as a function of ductility.

Time-history motions, compatible with Eurocode 8 response spectra Type 1 and Type 2, for different types of soil, are taken into account for this study. Two hysteretic models are considered: a bilinear kinematic model (for which the total stress range is equal to twice the yield stress, so that the Bauschinger effect is included, as shown in Fig. 4-1) and a ring-spring (flag shape) model, as shown in Fig. 3-5.

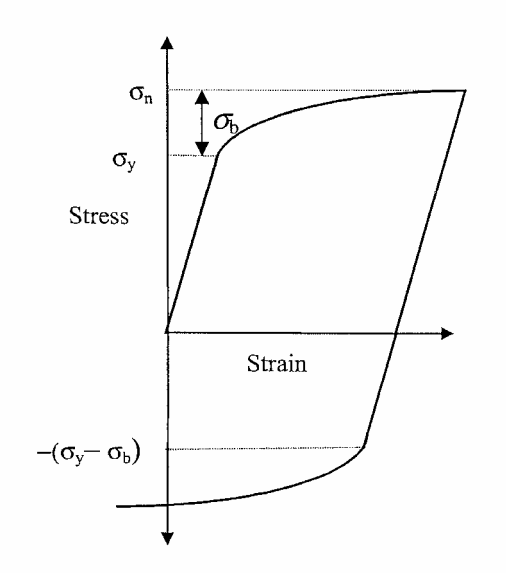


Fig. 4-1 Bilinear kinematic model with Bauschinger effect.

The first step of the procedure consisted in generating accelerograms compatible with Eurocode 8 response spectra.

## 4.1 Response Spectrum Compatible Accelerograms

Eurocode 8 compatible response spectra accelerograms were generated using the procedure described by Clough and Penzien (1993). As a first step, the power spectrum is derived from the given elastic acceleration response spectrum. From this power spectrum, a stationary waveform is obtained, which is further converted to nonstationary, by multiplying it with a deterministic time modulating function representative of the characteristics of the earthquake considered. The obtained signal is then adjusted, using the Fast Fourier Transform and the Inverse Fast Fourier Transform, in order to obtain an accelerogram that closely matches the specified displacement response spectrum. The procedure was implemented in the Cast3m (Millard, 1993) computer code.

The modulating function is shown in Fig. 4-2 (Jennings et. al., 1968), and is described by the following expressions:

$$\begin{array}{lllll} \text{Rise time } t_1 & t \le t_1 & \Rightarrow & f(t) = \left[\dfrac{t}{t_1}\right]^2 \\ \text{Strong motion duration} & t_1 < t < t_2 & \Rightarrow & f(t) = 1 \\ \text{Decay time} & t \ge t_2 & \Rightarrow & f(t) = e^{-2(t-t_2)} \end{array} \qquad (4.1)$$

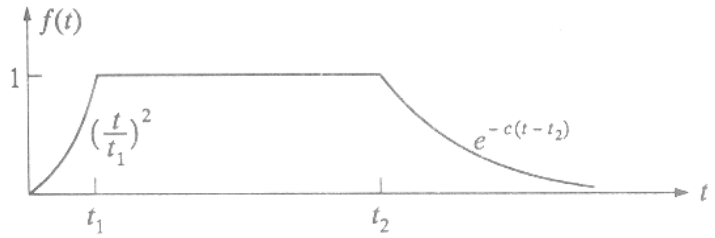


Fig. 4-2 Modulating function

The most important parameter in defining the modulating function is the strong motion duration, which represents the time period in which the motion power is almost constant near its maximum. Different authors have proposed empirical relationships for the strong motion duration.

The elastic response spectra given in Eurocode 8 may be classified as Type 1 or Type 2, depending on the surface wave magnitude; Type 2 spectrum is recommended for low magnitude earthquakes, up to a magnitude of 5.5. The formula expression proposed by Dobry et al. (1978) was considered for the computation of the strong motion duration as a function of magnitude *M*:

$$t_d = 10^{(0.43M - 1.83)} \quad \text{[sec]} \qquad (4.2)$$

This formula is valid for magnitudes between 4.5 and 7.6.

For each type of response spectrum, three different magnitudes were considered, associated to three different time intervals of the modulating function. The values of rise time $t_1$, strong motion duration ($t_2$-$t_1$) and total duration $t_{total}$ of the modulating function, are shown in Table 4-1, in terms of the magnitude considered.

Table 4-1 Characteristic time intervals

| Magnitude | $t_1$ | $t_2$-$t_1$ | $t_{total}$ |
|---|---|---|---|
| | *[sec]* | | |
| | **Type 1** | **Elastic response spectrum** | |
| **7.5** | 4 | 25 | 60 |
| **7.0** | 4 | 15 | 50 |
| **6.5** | 4 | 10 | 40 |
| | **Type 2** | **Elastic response spectrum** | |
| **5.5** | 2 | 4 | 30 |
| **5.0** | 2 | 3 | 25 |
| **4.5** | 2 | 2 | 20 |

For each of the five soil types (A through E) given in Eurocode 8 and for the six selected magnitudes, two accelerograms were generated. Thus, a total of 60 accelerograms compatible with Type 1 and Type 2 elastic response spectrum from Eurocode 8 were generated to determine the parameters of the linear equivalent system for each of the considered hysteretic models.

The elastic displacement spectrum $S_{De}(T)$ in Eurocode 8 may be obtained by direct transformation of the elastic acceleration response spectrum $S_e(T)$:

$$S_{De}(T) = S_e(T)\left[\frac{T}{2\pi}\right]^2 \tag{4.3}$$

Eurocode 8 recommends using this expression for vibration periods not exceeding 4.0 s.

For structures with vibration periods longer than 4.0 s, an expression for deriving the Type 1 elastic displacement response spectrum is presented in Informative Annex A of Eurocode 8.

Up to a period of vibration $T_E$, between 4.5 and 6.0 s (depending on the soil type) the spectral ordinates of the displacement spectrum are obtained from $S_e(T)$ considering Equation (4.3). For vibration periods beyond $T_E$, the ordinates of the elastic displacement response spectrum are obtained from the equations proposed in Annex A of Eurocode 8:

$$\begin{aligned} &T_E \le T \le T_F : S_{De}(T) = 0.025\, a_g S T_C T_D \left[2.5\eta + \left(\frac{T - T_E}{T_F - T_E}\right)(1 - 2.5\eta)\right] \\ &T \ge T_F : S_{De}(T) = 0.025\, a_g S T_C T_D \end{aligned} \tag{4.4}$$

in which $a_g$ is the design ground acceleration, $S$ is the soil factor, $\eta$ is the damping correction factor (equal to 1.00 for 5% viscous damping), $T_C$ and $T_D$ are reference vibration periods given by Eurocode 8 as a function of the soil type, and $T_F$ = 10.0 s is the vibration period from which the elastic structural displacement equals the ground displacement.

Note that there is a discrepancy for the displacement computed at period $T_E$ from Equation (4.4), as shown in Fig. 4-3 for the $S_{De}/a_g$ spectrum for soil A:

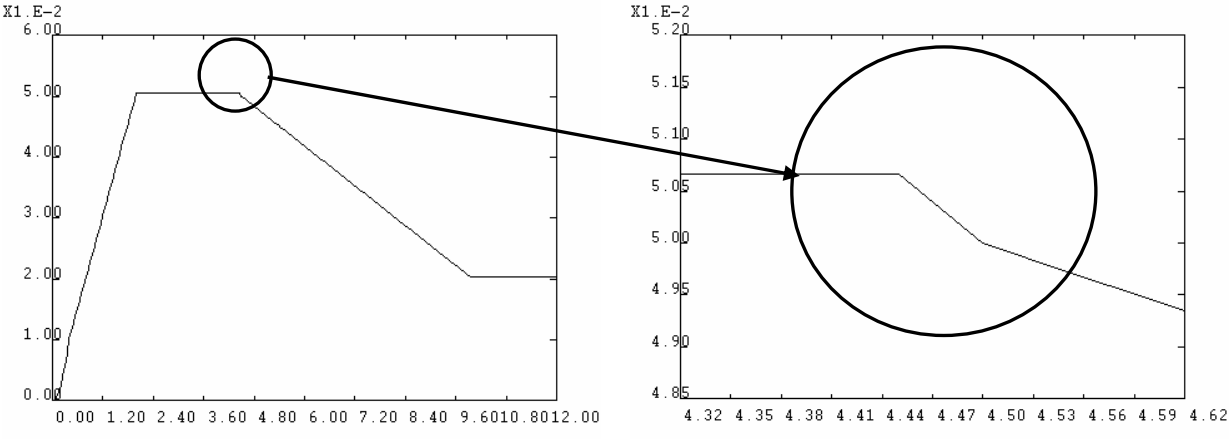


Fig. 4-3 Discrepancy in Type 1 elastic displacement response spectrum in EC8

This discrepancy comes from the approximation made in these equations, where:

$$\left[\frac{1}{2\pi}\right]^2 \cong 0.025 \tag{4.5}$$

For consistency, the exact value of $\left[\frac{1}{2\pi}\right]^2$ was considered in Equation (4.4).

The procedure proposed in this study for equivalent linearization considers a shift in the vibration period of the SDOF oscillator. According to Equation (3.11), which represents the expression of the equivalent period used by most of the equivalent linearization methods using a theoretical approach, the equivalent period may be up to 2.45 times greater than the initial period of the structure for a ductility ratio of 6. The present study is limited to structures with periods up to 4.0 s. Thus, considering the period shift, it is expected that for high ductility ratios the equivalent period may reach values up to 10.0 s. For this reason it is important that the response spectrum can give a correct estimation of elastic displacements at large periods of vibration, exceeding the values commonly used in design based on the reduction of the acceleration response spectrum.

No recommendation is given in Eurocode 8 to derive the Type 2 elastic displacement spectrum for vibration periods above 4.0 s. For the purpose of this study, it was considered that Equation (4.3) may be applied for Type 2 displacement spectrum up to a vibration period $T_E$ equal to 4.5 s, i.e., the minimum value considered for Type 1 displacement spectrum in Informative Annex A. As a result, the method proposed in the present study for Type 2 spectra will be limited to structures with vibration periods smaller than 4.0 s. The selection of the appropriate range of initial vibration periods considered for Type 2 spectra is described in Section 4.2.1.

## 4.2 Description of the Procedure and Results

The methodology for determining the equivalent period and damping follows the empirical approach of Iwan and Gates (1979, 1980), but instead of analysing a limited number of vibration periods and ductilities, a more refined procedure was set-up using the “SPON” procedure in Cast3m (Millard, 1993) computer code. This procedure calculates the inelastic displacement spectrum of a SDOF oscillator for a given hysteretic model and ductility ratio. Using this approach, a large set of models can be considered for a wide range of vibration periods and ductilities. For this study, vibration periods between 0 and 4.0 s at 0.02 s increments, and six ductility ratios (1.5, 2, 3, 4, 5 and 6) were considered.

As described in Section 3, Iwan and Gates (1979, 1980) observed that the overall shape of the inelastic PSV response spectrum of a SDOF oscillator for a given ductility ratio, resembles the shape of an elastic PSV spectrum shifted in period by some given factor. In the present procedure, the comparison was made at the level of elastic and inelastic displacement spectra. Thus, by making an estimation of the damping and period shift of the elastic spectra, for which the resulting displacements approximate with the smallest error the inelastic displacements, a set of "optimal" equivalent damping and equivalent period values may be obtained for each earthquake as a function of the ductility ratio. The procedure for determining the equivalent linearized properties of an inelastic system to earthquake excitation is described in the following section, using the bilinear kinematic model with 5% post-yielding to initial stiffness ratio and a Type 1 spectrum as a working example.

It is important to note that while Iwan and Gates (1979, 1980) derived equivalent properties considering the average of the results from six hysteretic models, in the present report, equivalent properties are derived separately for each one of the five hysteretic models (one bilinear kinematic and four ring-spring models) considered in the analysis.

### 4.2.1 Bilinear kinematic model

#### Type 1 compatible spectrum

The procedure is described by the following step-by-step algorithm:

1. For a given earthquake and ductility ratio, the inelastic displacement response spectrum $S_{Di}/a_g$ is determined. The value of the viscous damping ratio $\xi_0$ considered in the procedure is 5%. Fig. 4-4 shows the inelastic spectrum of a Type 1, 7.5 magnitude earthquake, considering type A soil conditions and a ductility ratio of 1.5.

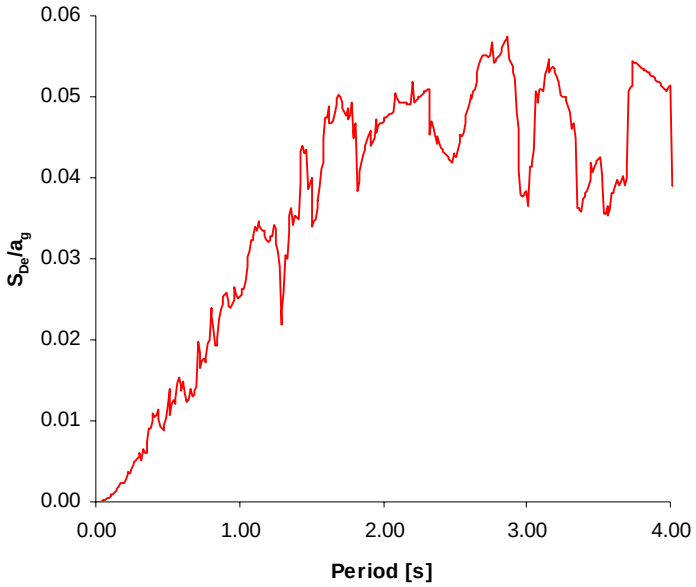


Fig. 4-4 Inelastic displacement spectra (Type 1, 7.5 Magnitude, Soil A; $\xi_0$ = 5%, $\mu$ = 1.5)

2. The elastic displacement response spectrum of the selected earthquake is calculated for damping ratios varying between 5 and 25% at 0.01% increments, with shifts of the initial period between 1 and 3 s at 0.01 s increments. The upper bound values in damping ratio and period shift were established after preliminary simulations performed with the largest value of ductility. Fig 4-5 shows the elastic displacement response spectrum $S_{De}/a_g$ for a damping ratio of 5%, compatible with the EC8 Type 1 response spectrum for soil A.

   For a given combination of damping ratio $\xi_{eq}$ (equivalent damping) and shifted period $T_{eq}$ (equivalent period), the shifted "equivalent" elastic spectral displacement is computed, for vibration periods of a SDOF oscillator between 0.02 and 4 s, at 0.02 s

increments. The ratio between the inelastic "exact" displacement $S_{Di}$ and the equivalent elastic displacement $S_{De}$ is calculated, with the error estimation $\varepsilon_i$ of the difference between these two displacements expressed as:

$$\varepsilon_i(\xi_{eq};T_{eq}) = \frac{S_{De}}{S_{Di}} - 1 \tag{4.6}$$

The measure of the overall error for the entire range of vibration periods between 0.02 s and 4.0 s is given by the average error:

$$\varepsilon(\xi_{eq};T_{eq}) = \sqrt{\sum_{i=1}^{N} \frac{\varepsilon_i^2}{N}} \tag{4.7}$$

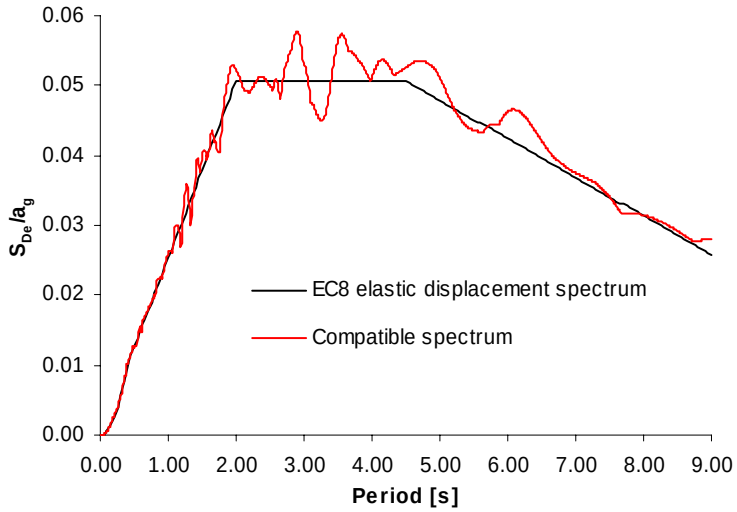


Fig. 4-5 Elastic displacement spectra (Type 1, 7.5 Magnitude, Soil A; $\xi_0$ = 5%)

where $N$ = 200 is the number of SDOF oscillators with vibration periods up to 4.0 s for which the inelastic and elastic shifted displacements are computed.

For a given ductility, the average error is calculated for all the possible combinations of $\xi_{eq}$ and $T_{eq}$. The pair ($\xi_{eq}$ ;$T_{eq}$) corresponding to the minimum value $\varepsilon_{min}$ ($\xi_{eq}$ ;$T_{eq}$) is retained, and defines the parameters of the equivalent linear system that gives the best approximation of inelastic displacement for the considered range of periods.

For example, considering the 7.5 magnitude earthquake compatible with the EC8 Type 1 spectrum for soil A, the following optimal parameters were determined for a ductility ratio of 1.5:

$\xi_{eq}$ = 6.25% and $T_{eq}$ =1.09$T_0$

in which $T_0$ is the initial period of the SDOF oscillator considered. For this pair of optimal values, the corresponding average error is equal to 12.5%. Fig. 4-6 shows the inelastic "exact" and the elastic equivalent displacement spectra calculated considering these optimal equivalent damping and period shift values.

Fig. 4-7 shows the average minimum error in terms of the ductility ratio, computed for the 30 earthquakes compatible with Type 1 spectra, considering the bilinear kinematic model. It can be observed that the errors range approximately between 10 and 30% and are increasing with ductility.

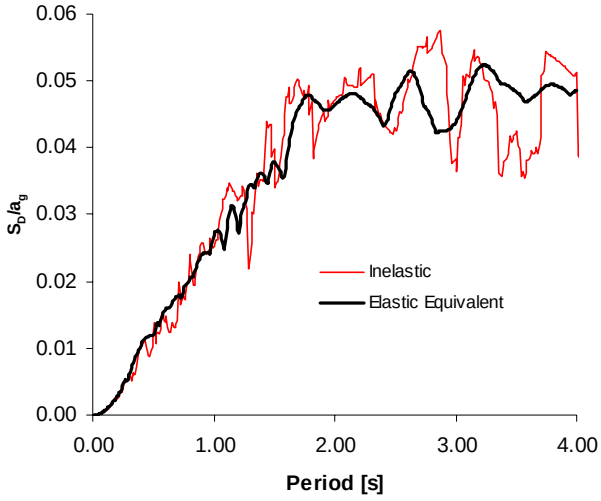


Fig. 4-6 Comparison between inelastic and equivalent elastic displacement spectrum

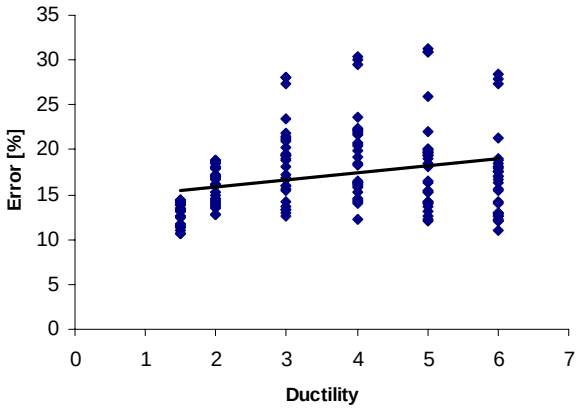


Fig. 4-7 Type 1 | Bilinear kinematic: Average error

3. The values of optimal period shift are plotted in Fig. 4-8 against the ductility ratio for all the 30 earthquakes compatible with Type 1 spectra, while in Fig. 4-9, the optimal damping ratio versus optimal period shift is plotted for all earthquakes and ductilities.

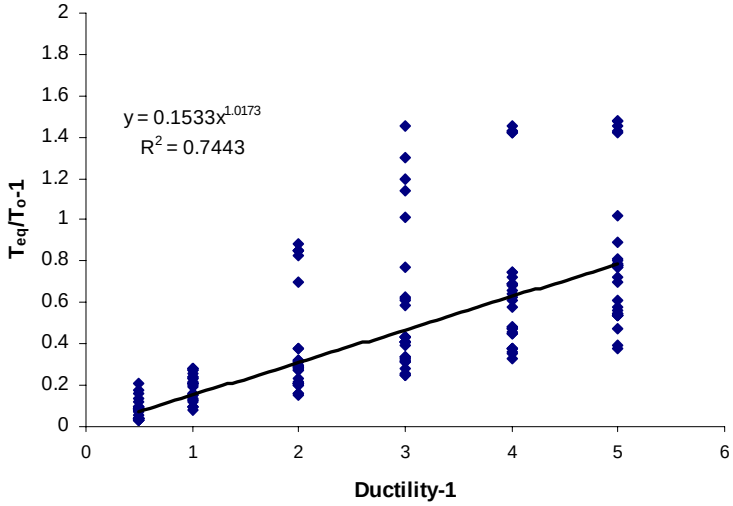


Fig. 4-8 Type 1 | Bilinear kinematic: Optimal period shift versus ductility

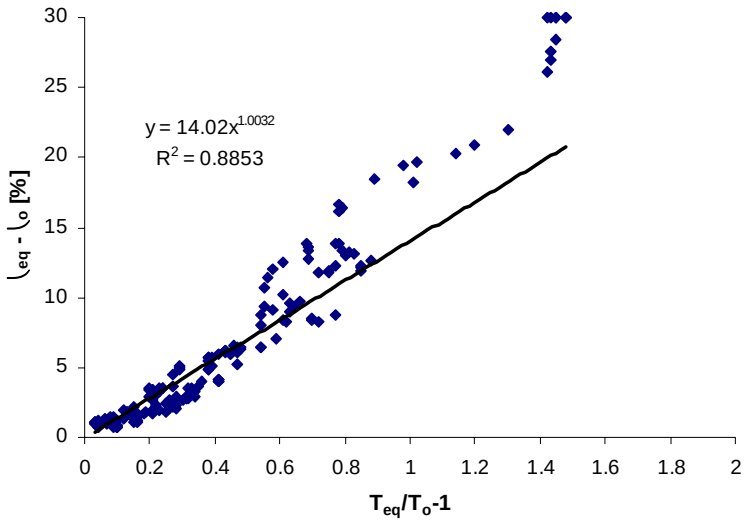


Fig. 4-9 Type 1 | Bilinear kinematic: Equivalent damping versus period shift

The trend lines of the scatter are given in both figures. A power-type function was considered for the trend lines. The optimal equivalent period may be expressed as a function of the ductility ratio and the initial period by the following equation:

$$\left(\frac{T_{eq}}{T_0}-1\right)=0.153\left(\mu-1\right)^{1.02} \quad \Rightarrow \quad T_{eq}=T_0\left[1+0.153\left(\mu-1\right)^{1.02}\right] \quad \text{[sec]} \tag{4.8}$$

while the equivalent damping function of period shift may be expressed as:

$$\xi_{eq}-\xi_0=14.0\left(\frac{T_{eq}}{T_0}-1\right)^{1.00} \quad \text{[\%]} \tag{4.9}$$

By replacing Equation (4.8) into Equation (4.9), the equivalent damping ratio is expressed as a function of the ductility ratio:

$$\xi_{eq}=\xi_0+2.14\left(\mu-1\right)^{1.02} \quad \text{[\%]} \tag{4.10}$$

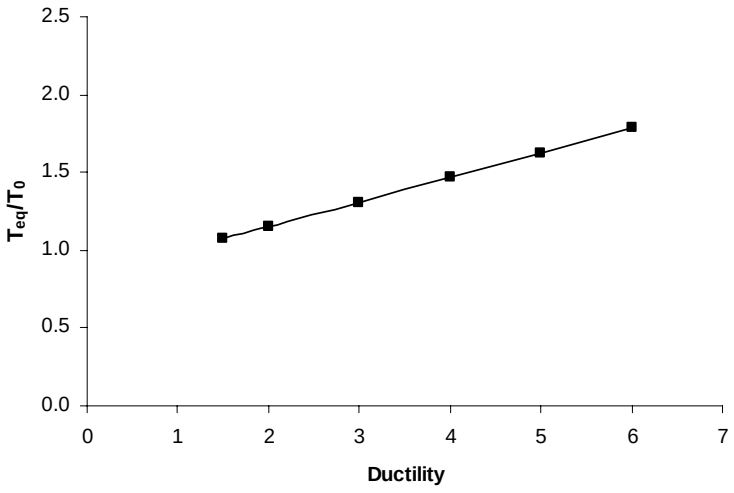


Fig. 4-10 Type 1 | Bilinear kinematic: Equivalent period versus ductility

Equations (4.8) and (4.10) give the parameters of the linear equivalent system as a function of the ductility ratio and the initial stiffness. Fig. 4-10 and Fig. 4-11 show, respectively, the evolution of equivalent period and damping as a function of ductility.

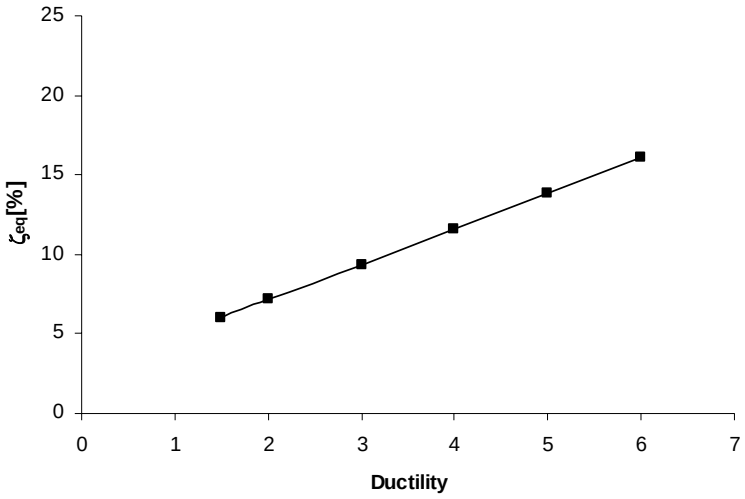


Fig. 4-11 Type 1 | Bilinear kinematic: Equivalent damping versus ductility

The ratio of approximate elastic displacements, determined using these formulas, to the exact inelastic displacements was computed, in order to investigate the accuracy of the procedure. The results for all 30 earthquakes were averaged for each ductility ratio and plotted for the range of periods between 0.02 and 4.0 s, as shown in Fig. 4-12. Generally, the errors are increasing with the level of ductility. Fig. 4-13 shows the ratios obtained by averaging all ductilities, together with the linear trend line of this characteristic. It may be observed that the procedure underestimates the exact displacement up to period values of about 2.3 s, and overestimates the exact displacement above this period. Because for short periods, below 0.1 seconds, the methodology produces high errors, the vibration period interval used for computing the trend line of Fig. 4-13 was limited to 0.1 - 4.0 s.

Fig. 4-14 shows the standard deviation function of the vibration period for all ductilities considered in the analysis. The standard deviation is generally increasing with increasing ductility.

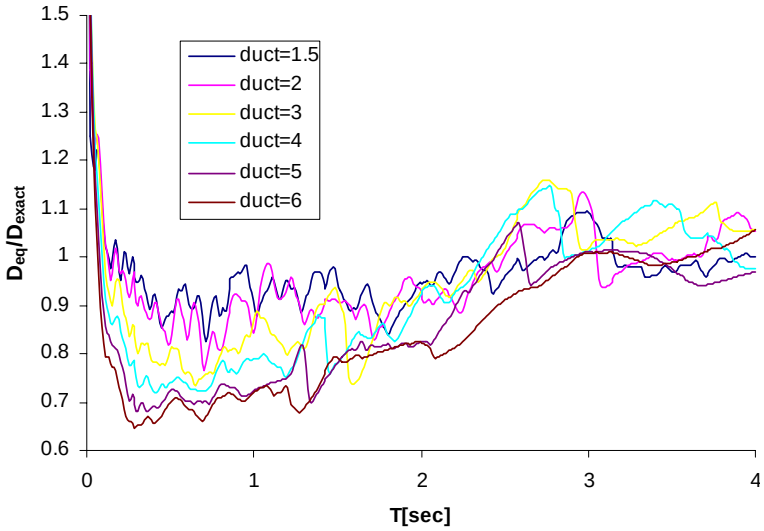


Fig. 4-12 Type 1 | Bilinear kinematic: Design to exact displacement (all $\mu$)

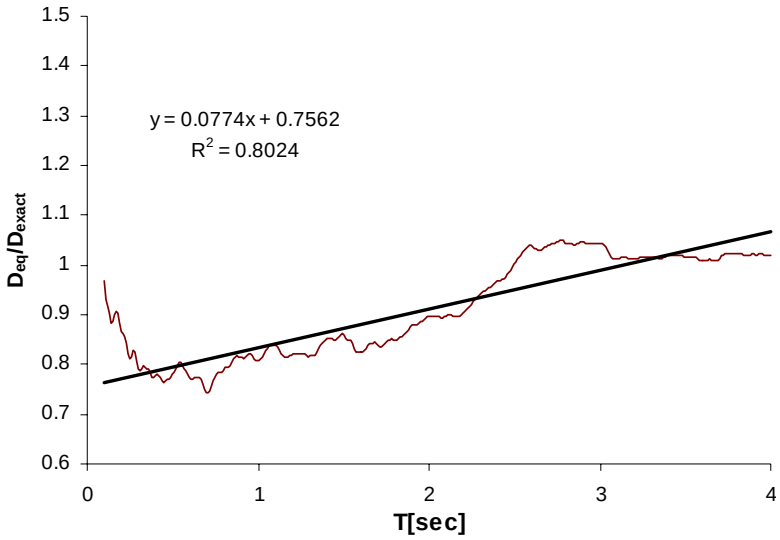


Fig. 4-13 Type 1 | Bilinear kinematic: Design to exact displacement (average $\mu$)

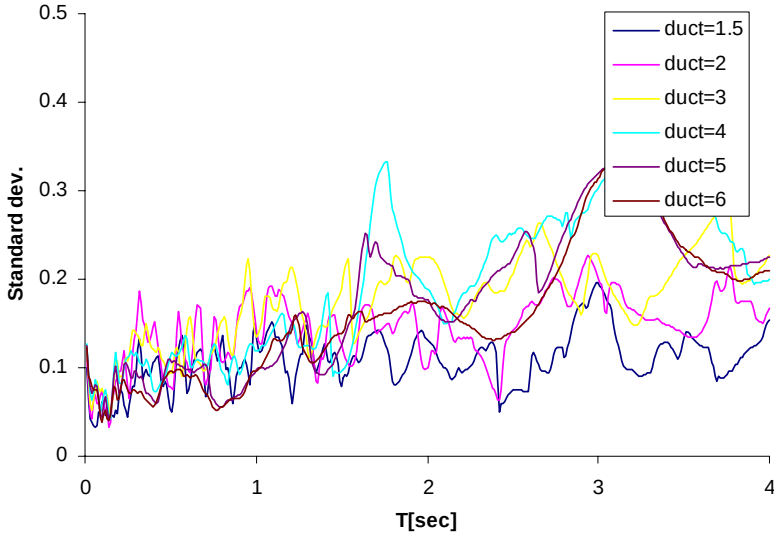


Fig. 4-14 Type 1 | Bilinear kinematic: Standard deviation

## Type 2 compatible spectrum

Fig. 4-15 through Fig. 4-22 show the steps and the results of the procedure for determining the equivalent period and damping for the elasto-plastic hysteretic model, considering a Type 2 compatible spectrum. The significance of the figures was explained above. The resulting equations for equivalent period and damping are:

$$T_{eq} = T_0 \left[ 1 + 0.252 \left( \mu - 1 \right)^{0.719} \right] \tag{4.11}$$

$$\xi_{eq} = \xi_0 + 3.35 \left( \mu - 1 \right)^{0.873} \quad [\%] \tag{4.12}$$

For the Type 2 elastic displacement spectrum, as explained in Section 4.1, a maximum vibration equivalent period of 4.5 s was considered in the analysis. Thus, the range of vibration periods $T_0$ of the SDOF oscillator for which the equations of equivalent period and damping are appicable depends on the period shift, as determined from Equation (4.11). Equation (4.13) shows an approximate relationship for determining the maximum vibration period of the SDOF oscillator for which the procedure may be applied. The procedure underestimates the exact displacement up to periods of about 1.2 s.

$$T_{0\max} = 4.5\,\mu^{-0.32} \le 4.0 \quad \text{[sec]} \tag{4.13}$$

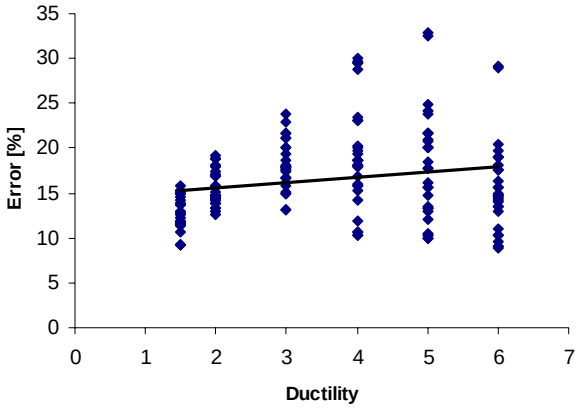


Fig. 4-15 Type 2 | Bilinear kinematic: Average error

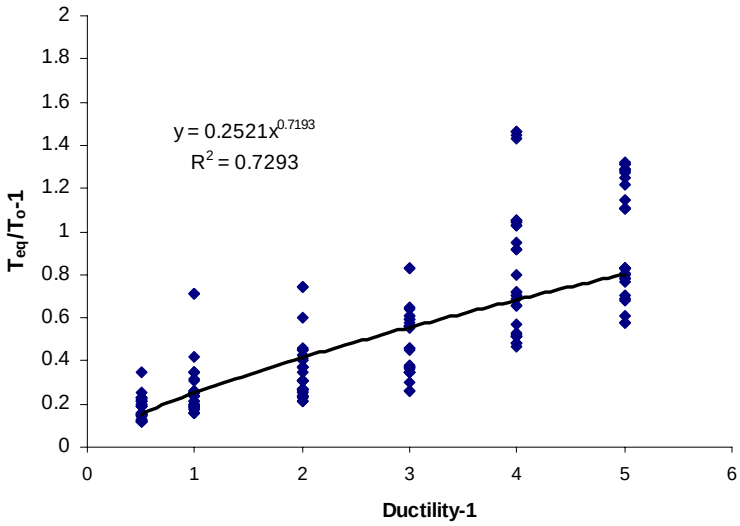


Fig. 4-16 Type 2 | Bilinear kinematic: Period shift versus ductility

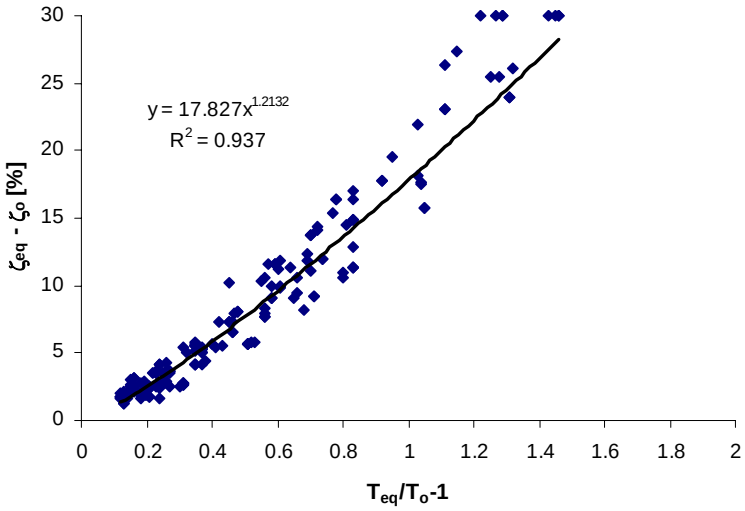


Fig. 4-17 Type 2 | Bilinear kinematic: Equivalent damping versus period shift

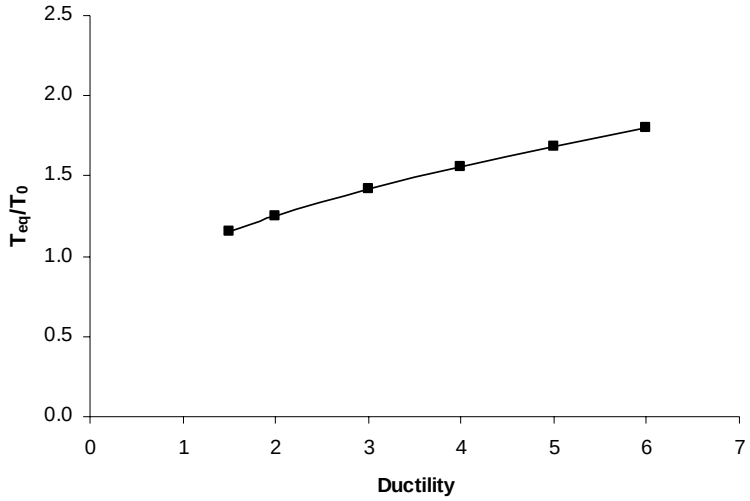


Fig. 4-18 Type 2 | Bilinear kinematic: Equivalent period versus ductility

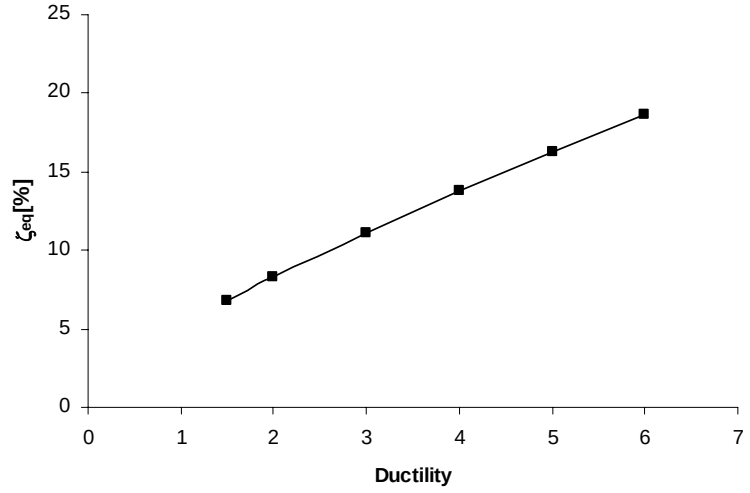


Fig. 4-19 Type 2 | Bilinear kinematic: Equivalent damping versus ductility

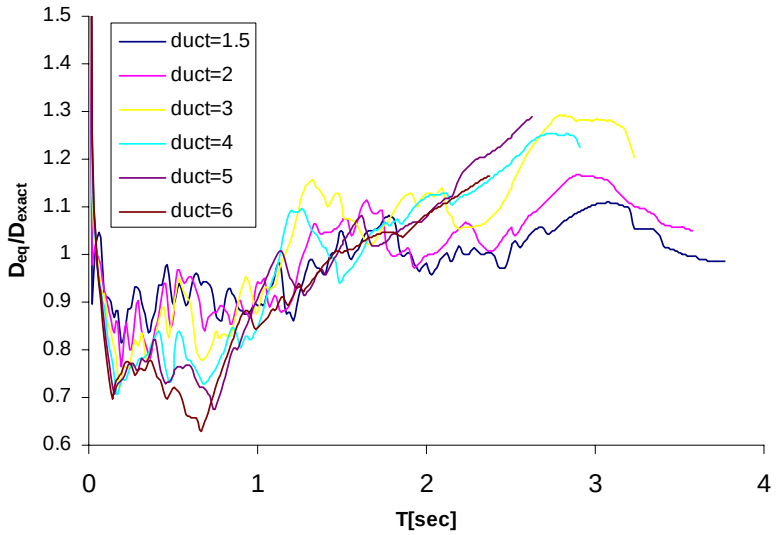


Fig. 4-20 Type 2 | Bilinear kinematic: Design to exact displacement (all $\mu$)

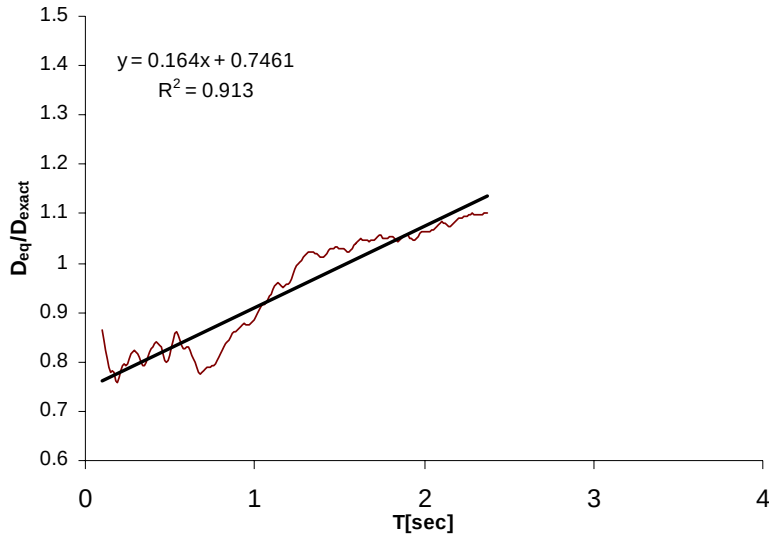


Fig. 4-21 Type 2 | Bilinear kinematic: Design to exact displacement (average $\mu$)

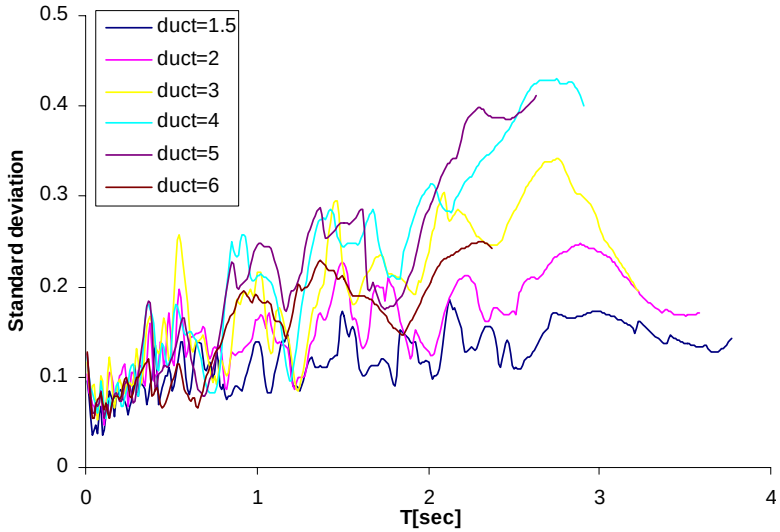


Fig. 4-22 Type 2 | Bilinear kinematic: Standard deviation

### 4.2.2 Ring-Spring hysteretic model

The ring-spring hysteretic model is shown in Fig. 3-5. The model can be used to model prestressed concrete with unbounded prestressed tendons (Blandon and Priestley, 2004, 2005) or bridges with insufficient detailing. This model is also suitable to model memory shape materials and is characterised by bilinear elastic response with low hysteretic damping. With reference to Fig. 3-5, the model is described (Blandon, 2004) by the initial stiffness $K_0$, the post-elastic coefficient $r$, the unloading lower stiffness coefficient $r_{lower}$ and the ratio $R = F_0/F_y$. The following formulas correspond to the ring-spring hysteretic model:

$$R = \frac{F_0}{F_y} = \frac{r_{lower}}{r}\frac{1-r}{1-r_{lower}} \tag{4.14}$$

$$r_{lower} = \frac{Rr}{1-r+Rr} \tag{4.15}$$

Equation (4.14) is used to determine $R$ as a function of $r$ and $r_{lower}$, while Equation (4.15) is used to determine $r_{lower}$ as a function of $R$ and $r$. The following parameters were considered in the procedure for the ring-spring hysteretic model:

$R$ = 1/3, $r$ = 0.025 / 0.05 / 0.1 (most common for bridges with insufficient detailing);

$R$ = 2/3, $r$ = 0.05 (low damping).

A value of $r_{steep}$ = 1 was considered in all models, with equal tension and compression sides.

### Type 1 compatible spectrum | ($R$ = 1/3, $r$ = 0.025)

Fig. 4-23 through Fig. 4-30 show the steps and the results of the procedure for determining the equivalent period and damping for the ring-spring hysteretic model with $R$ = 1/3 and $r$ = 0.025 (resulting in $r_{low}$ = 0.00847), considering a Type 1 compatible spectrum. The equations for equivalent period and damping are expressed as:

$$T_{eq} = T_0 \left[ 1 + 0.159 \left( \mu - 1 \right)^{1.10} \right] \tag{4.16}$$

$$\xi_{eq} = \xi_0 + 3.66 \left( \mu - 1 \right)^{0.839} \quad [\%] \tag{4.17}$$

The procedure underestimates the exact displacement up to period values of about 2.2 s.

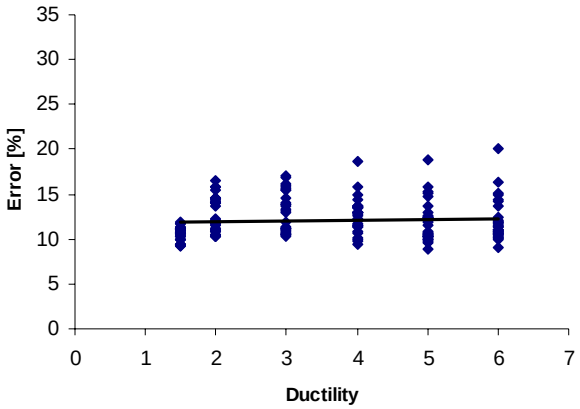


Fig. 4-23 Type 1 | Ring-spring ($R$ = 1/3, $r$ = 0.025): Average error

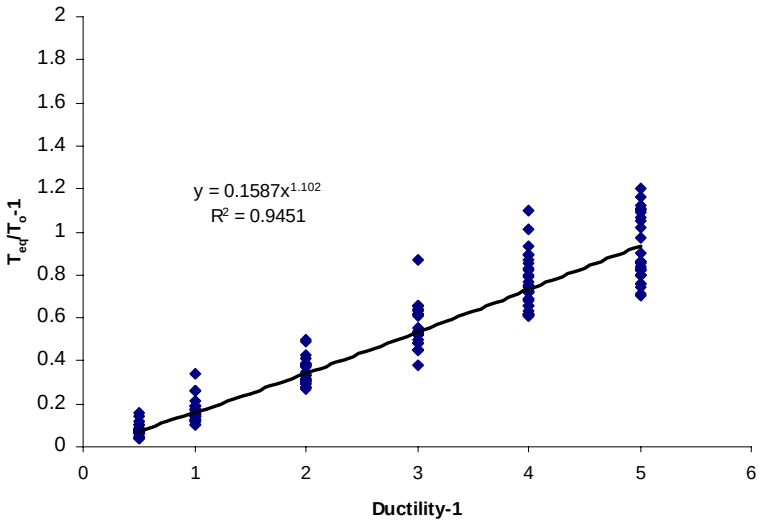


Fig. 4-24 Type 1 | Ring-spring ($R$ = 1/3, $r$ = 0.025): Period shift versus ductility

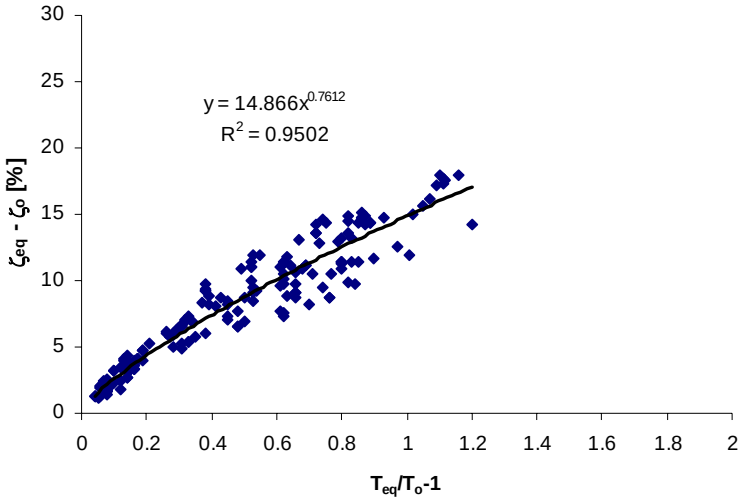


Fig. 4-25 Type 1 | Ring-spring ($R$ = 1/3, $r$ = 0.025): Equivalent damping versus period shift

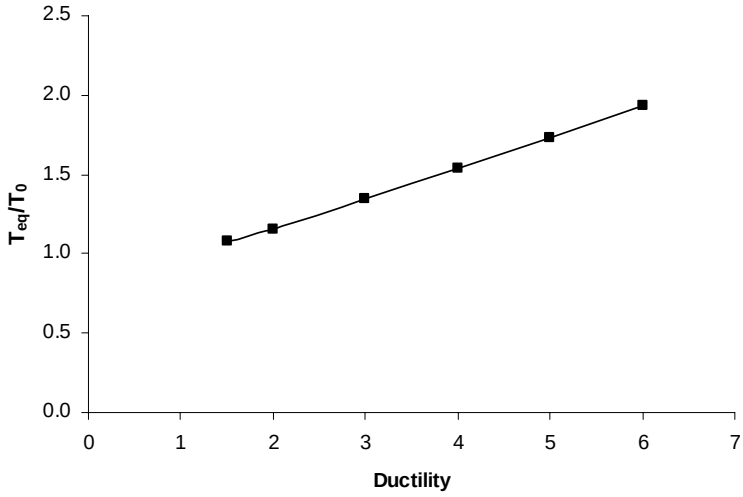


Fig. 4-26 Type 1 | Ring-spring ($R$ = 1/3, $r$ = 0.025): Equivalent period versus ductility

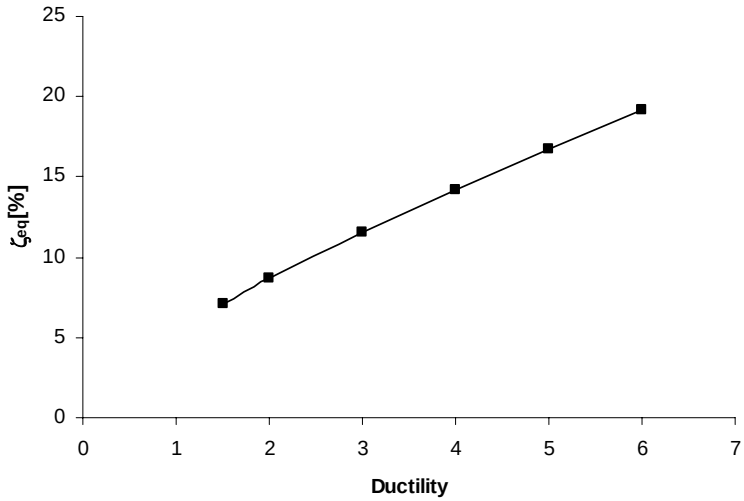


Fig. 4-27 Type 1 | Ring-spring ($R$ = 1/3, $r$ = 0.025): Equivalent damping versus ductility

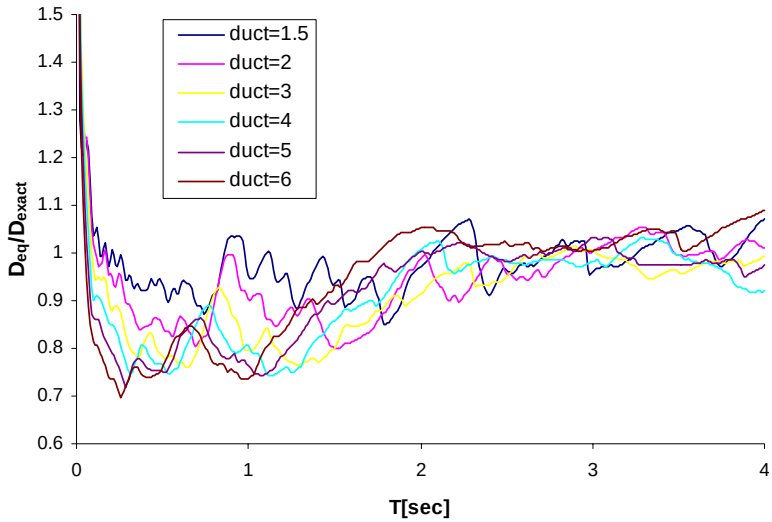


Fig. 4-28 Type 1 | Ring-spring ($R$ = 1/3, $r$ = 0.025): Design to exact displacement (all $\mu$)

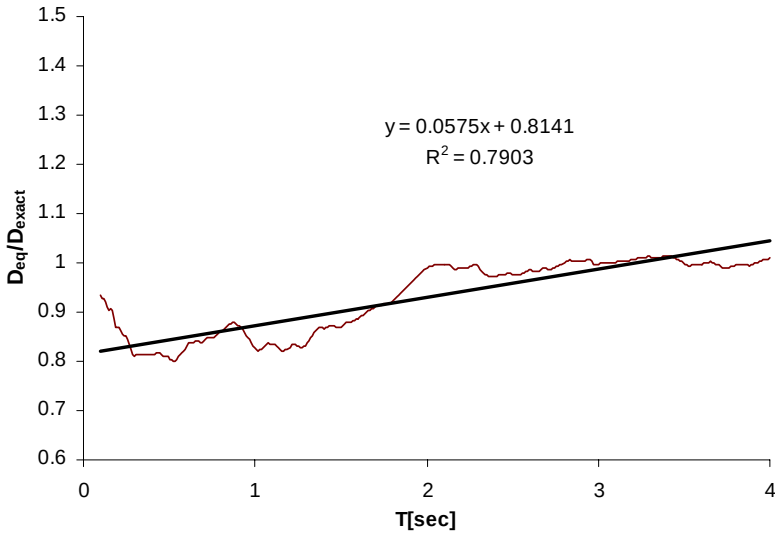


Fig. 4-29 Type 1 | Ring-spring ($R$ = 1/3, $r$ = 0.025): Design to exact displacement (average $\mu$)

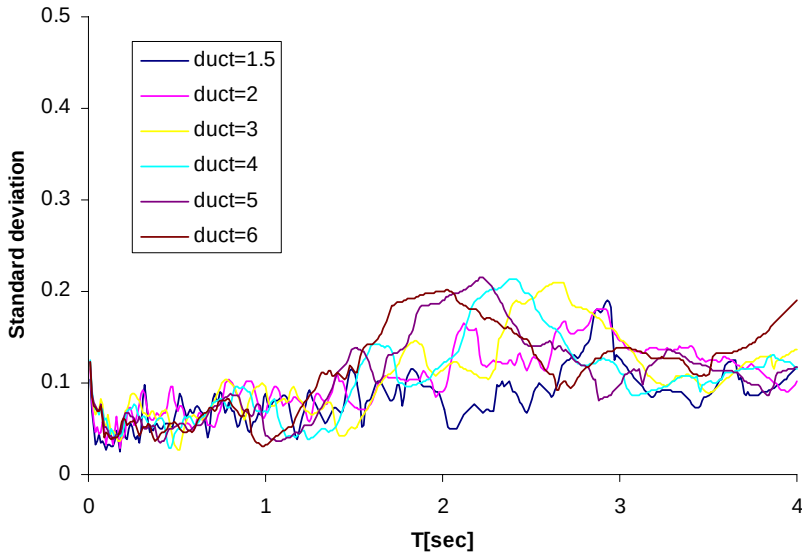


Fig. 4-30 Type 1 | Ring-spring ($R$ = 1/3, $r$ = 0.025): Standard deviation

### Type 2 compatible spectrum | (*R* = 1/3, *r* = 0.025)

Fig. 4-31 and Fig. 4-38 show the steps and the results of the procedure for determining the equivalent period and damping for the ring-spring hysteretic model with *R* = 1/3 and *r* = 0.025 (resulting in $r_{low}$ = 0.00847), considering a Type 2 compatible spectrum. The equations for equivalent period and damping are expressed as:

$$T_{eq} = T_0 \left[ 1 + 0.259 \left( \mu - 1 \right)^{0.748} \right] \tag{4.18}$$

$$\xi_{eq} = \xi_0 + 4.53 \left( \mu - 1 \right)^{0.657} \quad [\%] \tag{4.19}$$

The expression for determining the maximum vibration period of the SDOF oscillator for which the procedure is applicable is:

$$T_{0\max} = 4.5\, \mu^{-0.34} \leq 4.0 \quad [\text{sec}] \tag{4.20}$$

The procedure underestimates the exact displacement up to period values of approximately 1 s, and overestimates the exact displacement above this period.

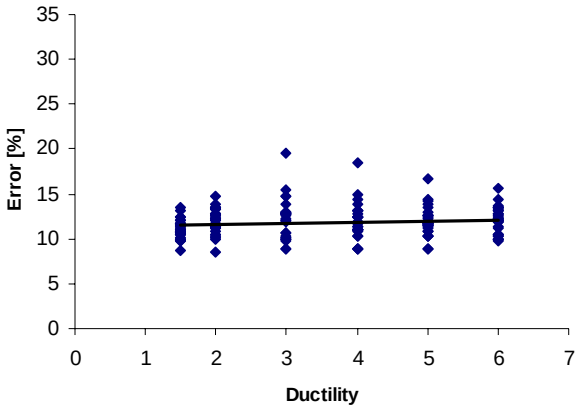


Fig. 4-31 Type 2 | Ring-spring (*R* = 1/3, *r* = 0.025): Average error

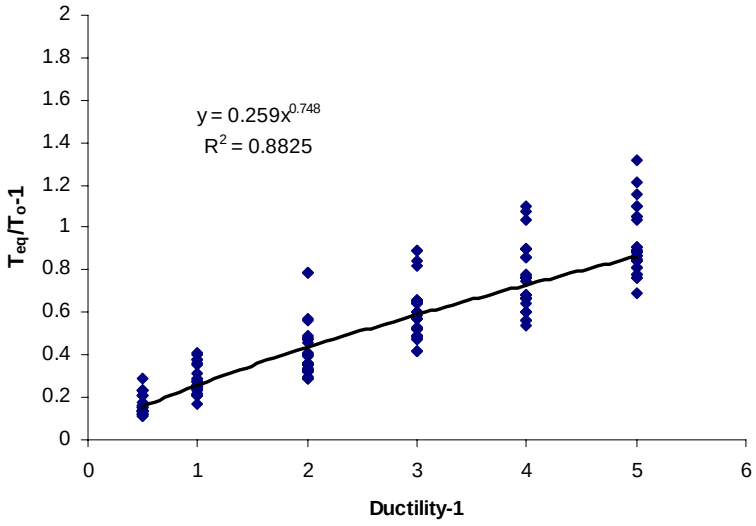


Fig. 4-32 Type 2 | Ring-spring (*R* = 1/3, *r* = 0.025): Period shift versus ductility

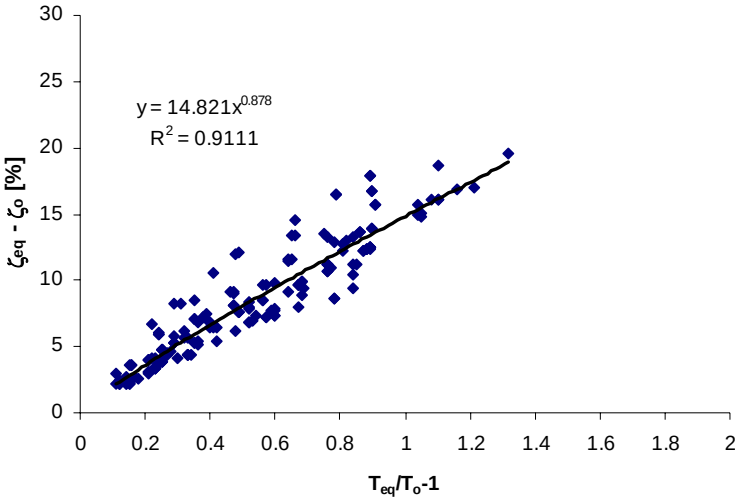


Fig. 4-33 Type 2 | Ring-spring (*R* = 1/3, *r* = 0.025): Equivalent damping versus period shift

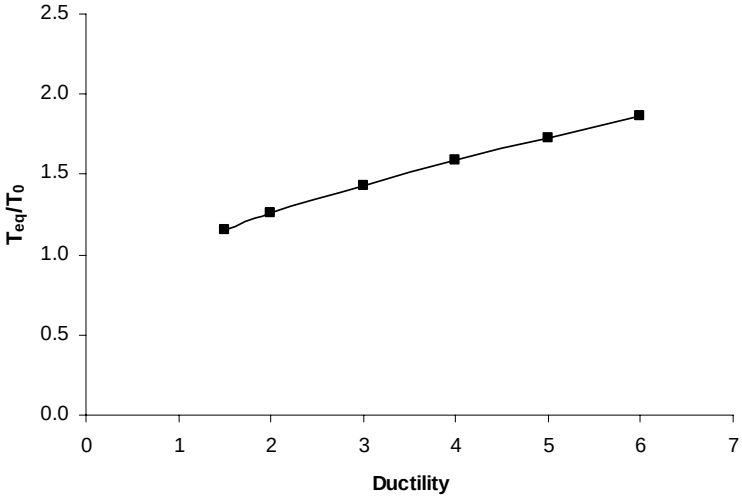


Fig. 4-34 Type 2 | Ring-spring (*R* = 1/3, *r* = 0.025): Equivalent period versus ductility

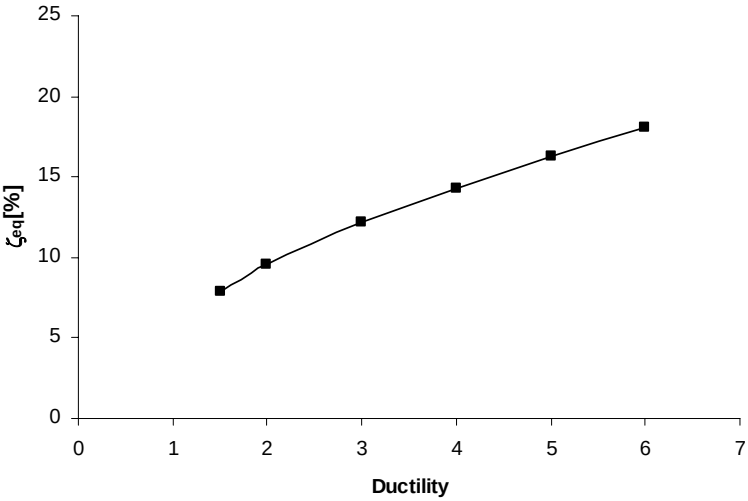


Fig. 4-35 Type 2 | Ring-spring (*R* = 1/3, *r* = 0.025): Equivalent damping versus ductility

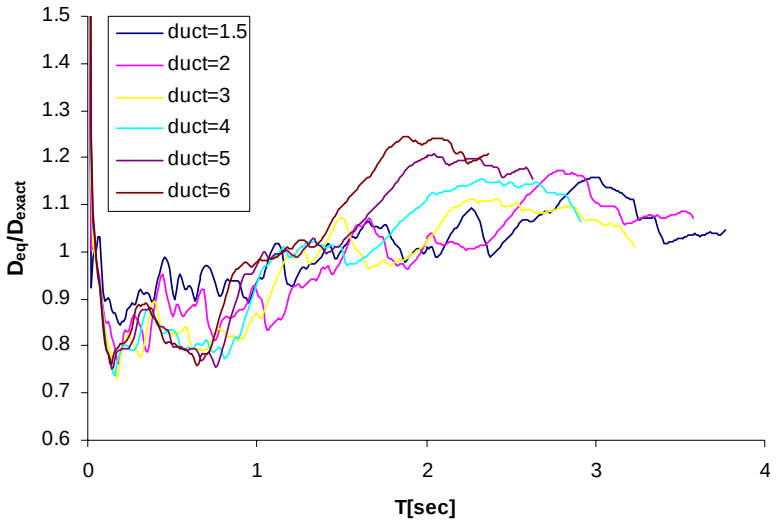


Fig. 4-36 Type 2 | Ring-spring ($R$ = 1/3, $r$ = 0.025): Design to exact displacement (all $\mu$)

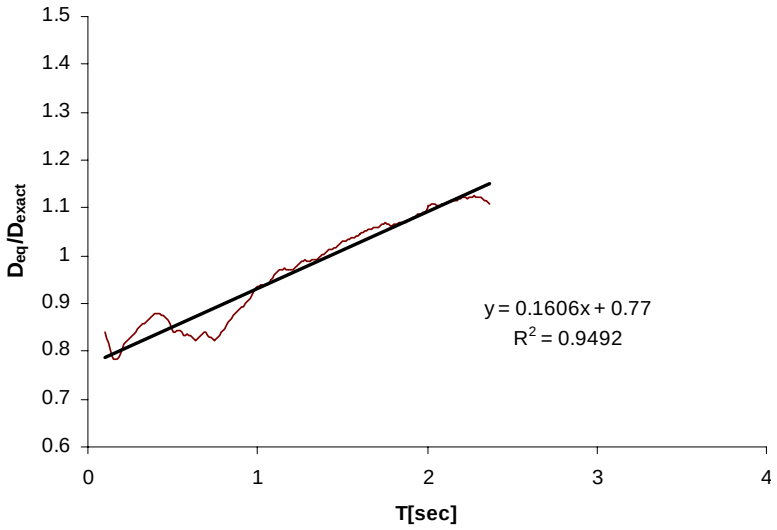


Fig. 4-37 Type 2 | Ring-spring ($R$ = 1/3, $r$ = 0.025): Design to exact displacement (average $\mu$)

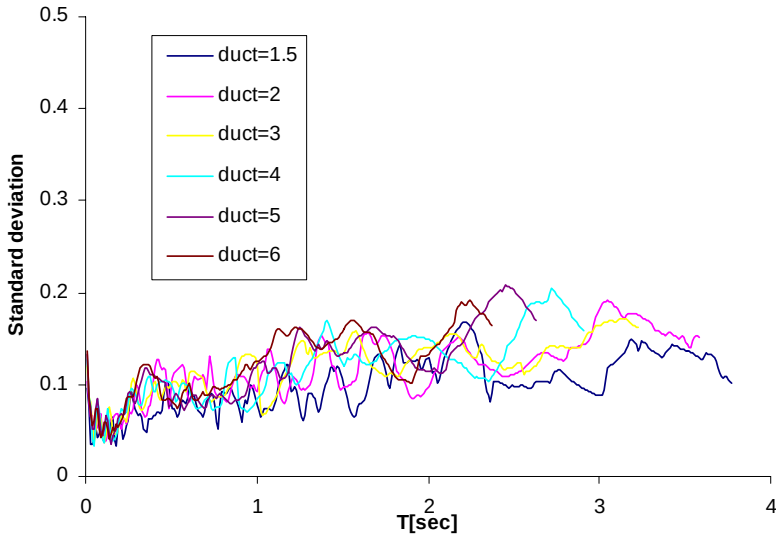


Fig. 4-38 Type 2 | Ring-spring ($R$ = 1/3, $r$ = 0.025): Standard deviation

### Type 1 compatible spectrum | (*R* = 1/3, *r* = 0.05)

Fig. 4-39 and Fig. 4-46 show the steps and the results of the procedure for determining the equivalent period and damping for the ring-spring hysteretic model with *R* = 1/3 and *r* = 0.05 (resulting in $r_{low}$ = 0.00172), considering a Type 1 compatible spectrum. The equations for equivalent period and damping are expressed as:

$$T_{eq} = T_0 \left[ 1 + 0.153 \left( \mu - 1 \right)^{1.10} \right] \tag{4.21}$$

$$\xi_{eq} = \xi_0 + 3.63 \left( \mu - 1 \right)^{0.842} \quad [\%] \tag{4.22}$$

The procedure generally underestimates the exact displacement up to period values of approximately 2 s.

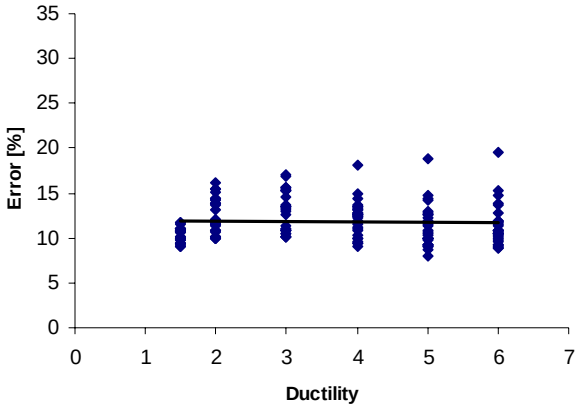


Fig. 4-39 Type 1 | Ring-spring (*R* = 1/3, *r* = 0.05): Average error

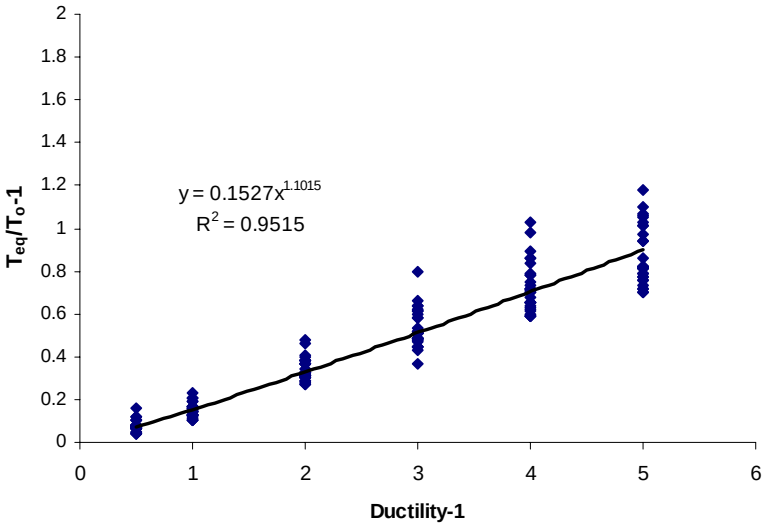


Fig. 4-40 Type 1 | Ring-spring (*R* = 1/3, *r* = 0.05): Period shift versus ductility

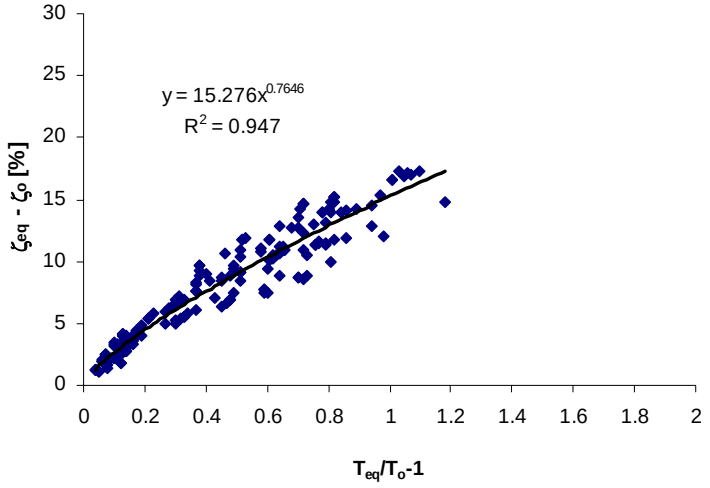


Fig. 4-41 Type 1 | Ring-spring (*R* = 1/3, *r* = 0.05): Equivalent damping versus period shift

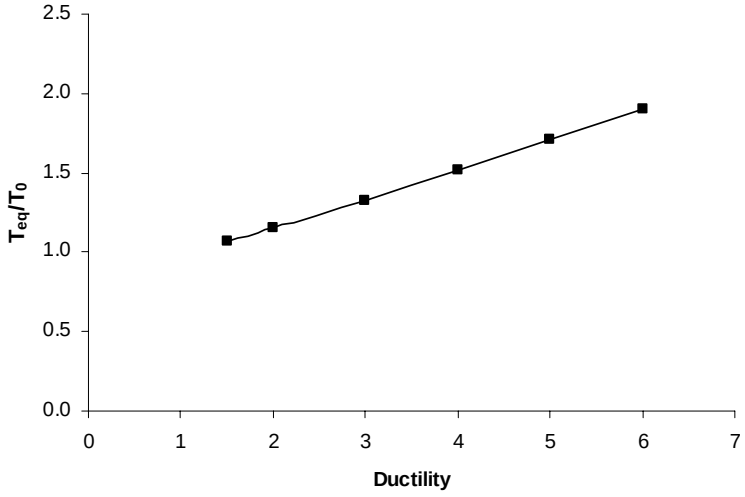


Fig. 4-42 Type 1 | Ring-spring (*R* = 1/3, *r* = 0.05): Equivalent period versus ductility

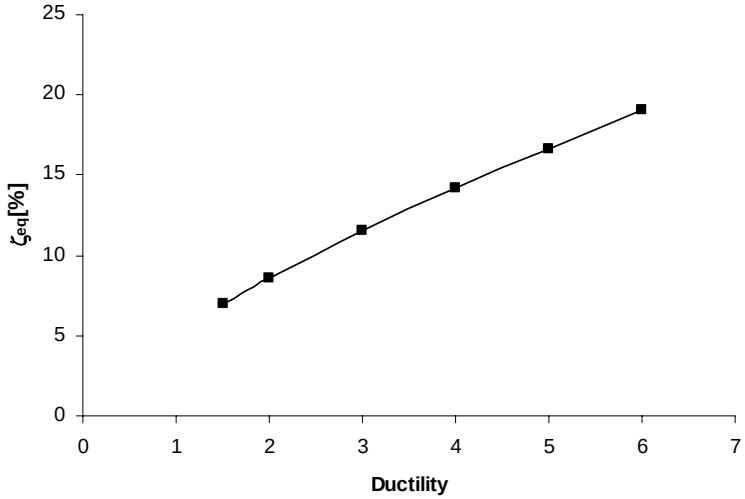


Fig. 4-43 Type 1 | Ring-spring (*R* = 1/3, *r* = 0.05): Equivalent damping versus ductility

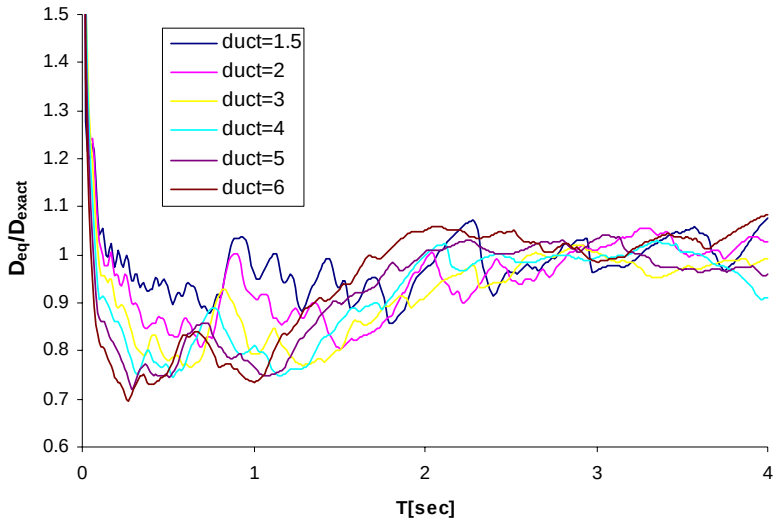


Fig. 4-44 Type 1 | Ring-spring ($R$ = 1/3, $r$ = 0.05): Design to exact displacement (all $\mu$)

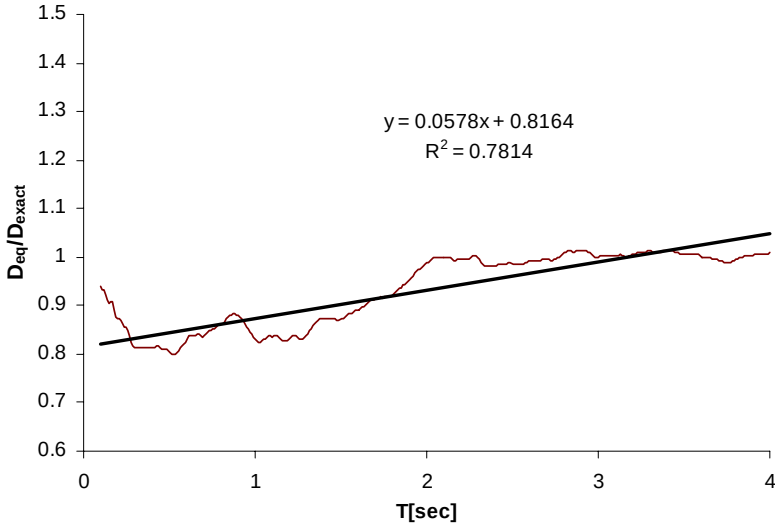


Fig. 4-45 Type 1 | Ring-spring ($R$ = 1/3, $r$ = 0.05): Design to exact displacement (average $\mu$)

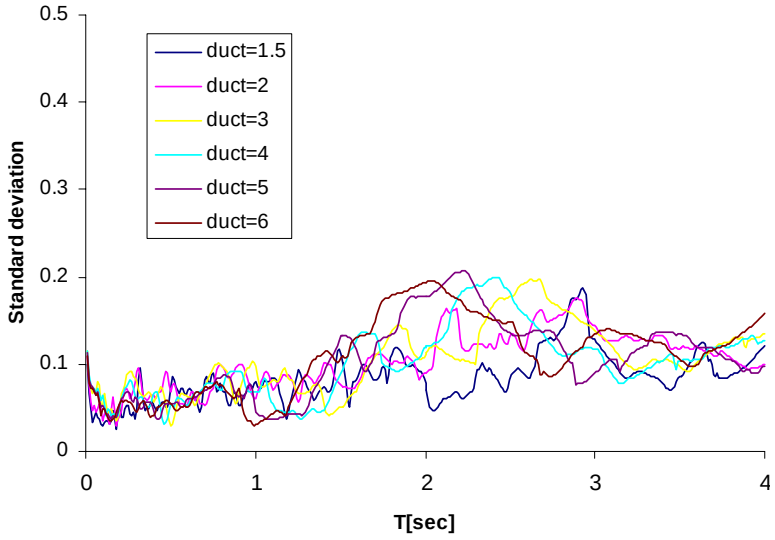


Fig. 4-46 Type 1 | Ring-spring ($R$ = 1/3, $r$ = 0.05): Standard deviation

### Type 2 compatible spectrum | (*R* = 1/3, *r* = 0.05)

Fig. 4-47 through Fig. 4-54 show the steps and the results of the procedure for determining the equivalent period and damping for the ring-spring hysteretic model with $R$ = 1/3 and $r$ = 0.05 (resulting in $r_{low}$ = 0.00172), considering a Type 2 compatible spectrum. The equations for equivalent period and damping are expressed as:

$$T_{eq} = T_0 \left[ 1 + 0.255 \left( \mu - 1 \right)^{0.726} \right] \tag{4.23}$$

$$\xi_{eq} = \xi_0 + 4.52 \left( \mu - 1 \right)^{0.650} \quad [\%] \tag{4.24}$$

The expression for determining the maximum vibration period of the SDOF oscillator for which the procedure is applicable is:

$$T_{0\max} = 4.5 \, \mu^{-0.33} \leq 4.0 \quad [\text{sec}] \tag{4.25}$$

The procedure underestimates the exact displacement up to period values of approximately 1.4 s, and overestimates the exact displacement above this period.

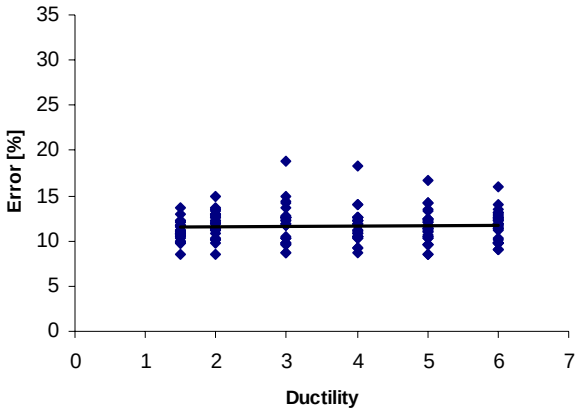


Fig. 4-47 Type 2 | Ring-spring (*R* = 1/3, *r* = 0.05): Average error

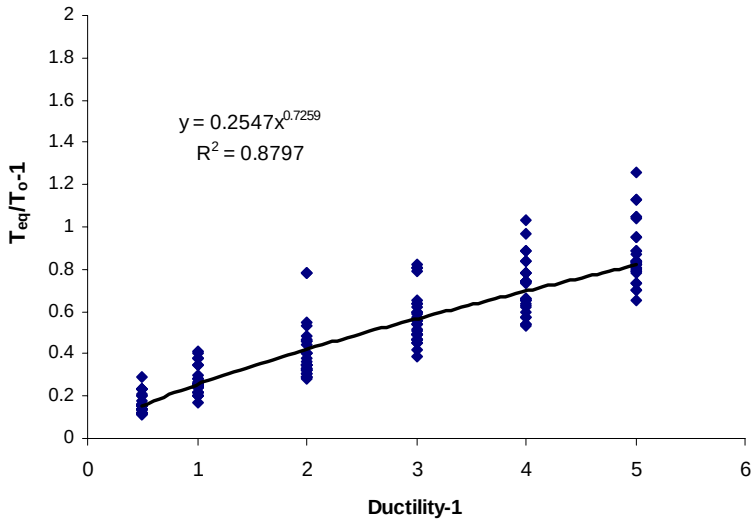


Fig. 4-48 Type 2 | Ring-spring (*R* = 1/3, *r* = 0.05): Period shift versus ductility

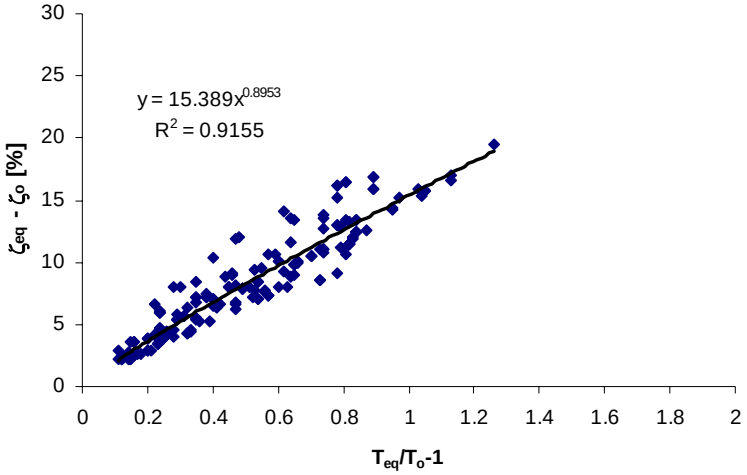


Fig. 4-49 Type 2 | Ring-spring (*R* = 1/3, *r* = 0.05): Equivalent damping versus period shift

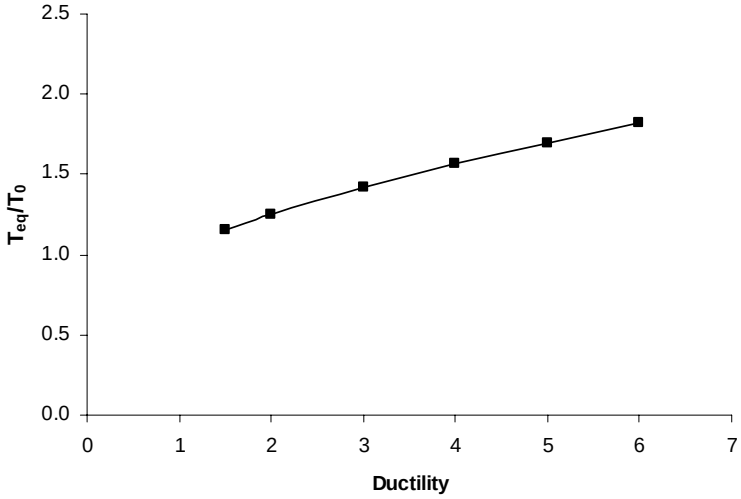


Fig. 4-50 Type 2 | Ring-spring (*R* = 1/3, *r* = 0.05): Equivalent period versus ductility

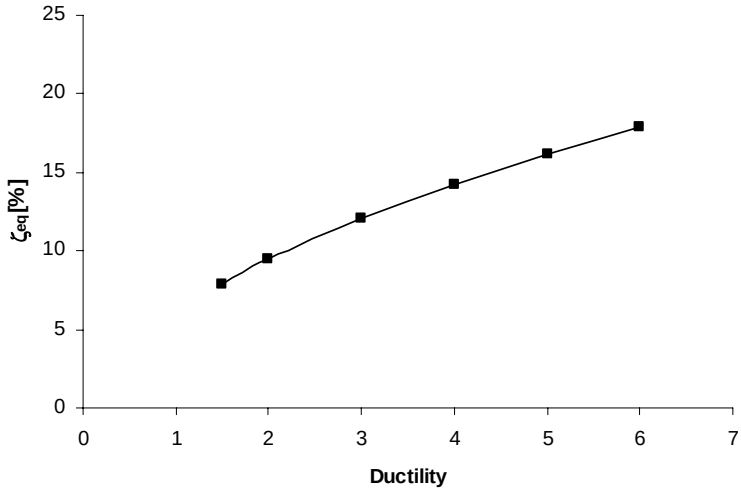


Fig. 4-51 Type 2 | Ring-spring (*R* = 1/3, *r* = 0.05): Equivalent damping versus ductility

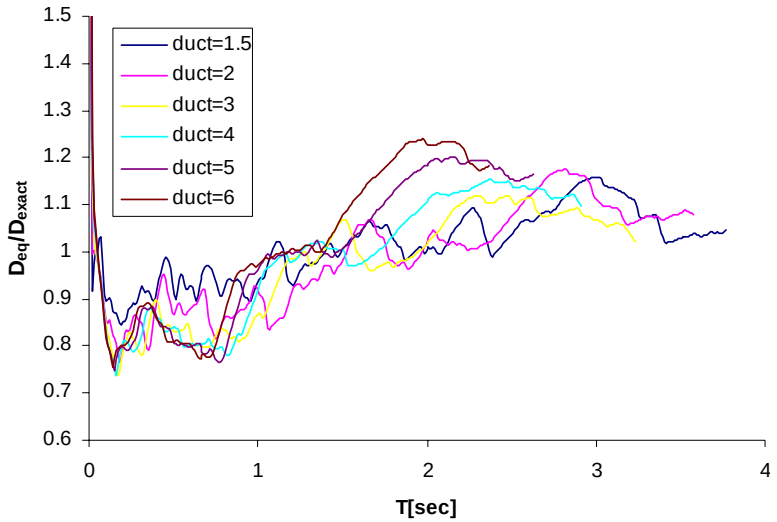


Fig. 4-52 Type 2 | Ring-spring ($R$ = 1/3, $r$ = 0.05): Design to exact displacement (all $\mu$)

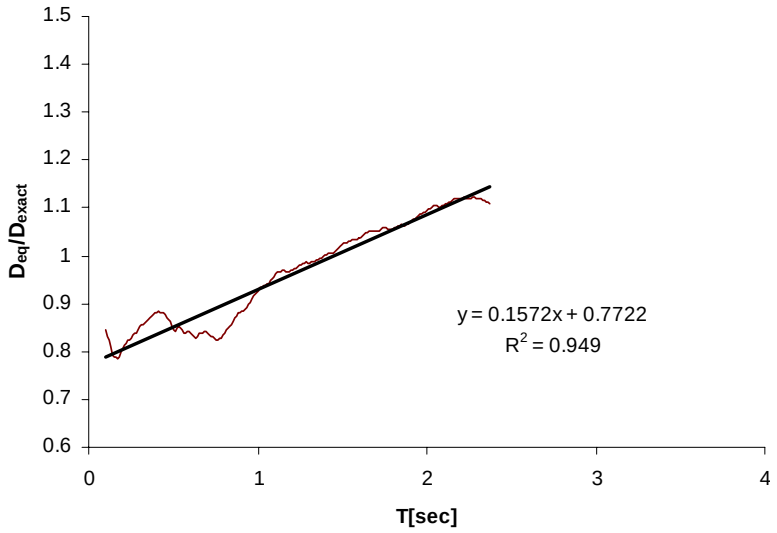


Fig. 4-53 Type 2 | Ring-spring ($R$ = 1/3, $r$ = 0.05): Design to exact displacement (average $\mu$)

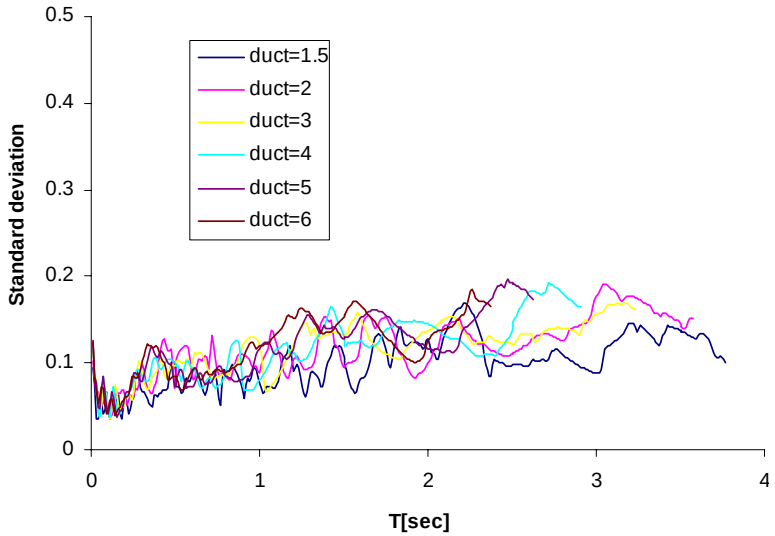


Fig. 4-54 Type 2 | Ring-spring ($R$ = 1/3, $r$ = 0.05): Standard deviation

### Type 1 compatible spectrum | (*R* = 1/3, *r* = 0.1)

Fig. 4-55 through Fig. 4-62 show the steps and the results of the procedure for determining the equivalent period and damping for the ring-spring hysteretic model with *R* = 1/3 and *r* = 0.1 (resulting in $r_{low}$ = 0.00357), considering a Type 1 compatible spectrum. The equations for equivalent period and damping are expressed as:

$$T_{eq} = T_0 \left[ 1 + 0.143 \left( \mu - 1 \right)^{1.07} \right] \tag{4.26}$$

$$\xi_{eq} = \xi_0 + 3.52 \left( \mu - 1 \right)^{0.845} \quad [\%] \tag{4.27}$$

The procedure generally underestimates the exact displacement up to period values of approximately 2 s.

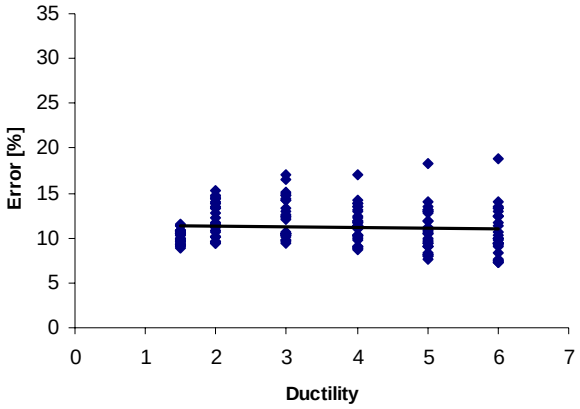


Fig. 4-55 Type 1 | Ring-spring (*R* = 1/3, *r* = 0.1): Average error

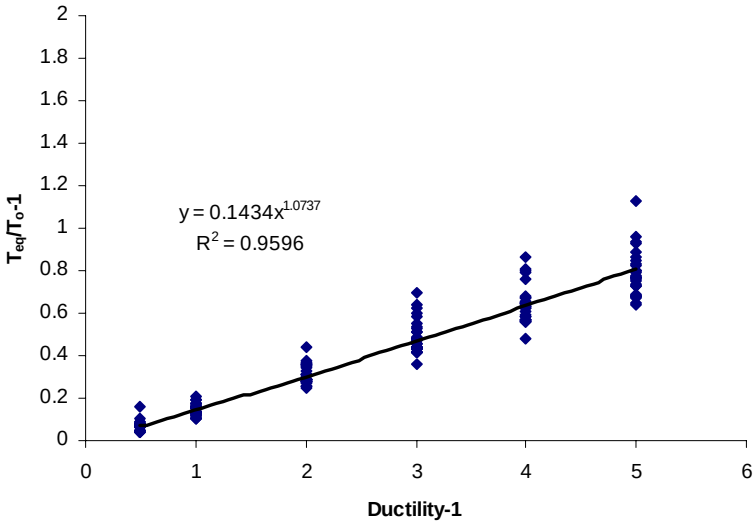


Fig. 4-56 Type 1 | Ring-spring (*R* = 1/3, *r* = 0.1): Period shift versus ductility

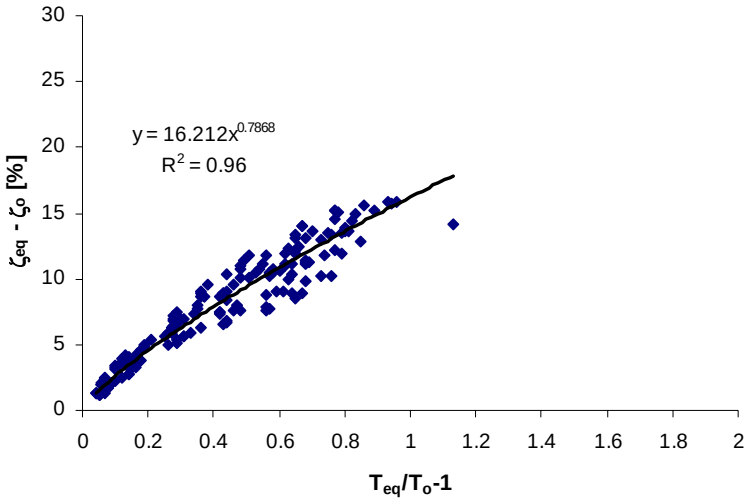


Fig. 4-57 Type 1 | Ring-spring (*R* = 1/3, *r* = 0.1): Equivalent damping versus period shift

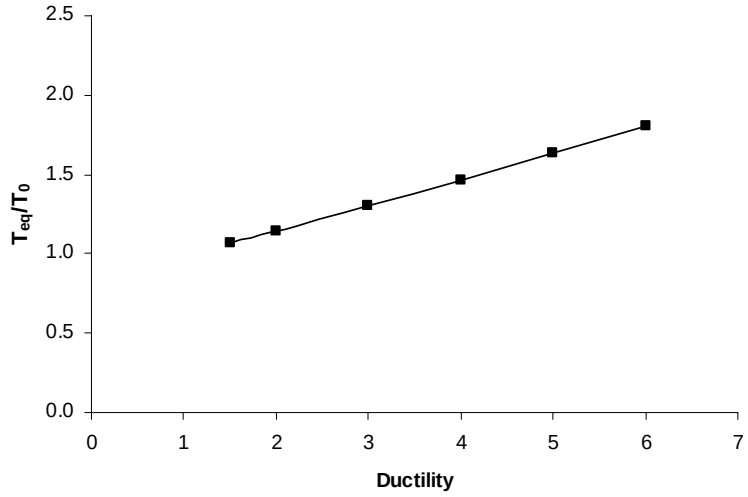


Fig. 4-58 Type 1 | Ring-spring (*R* = 1/3, *r* = 0.1): Equivalent period versus ductility

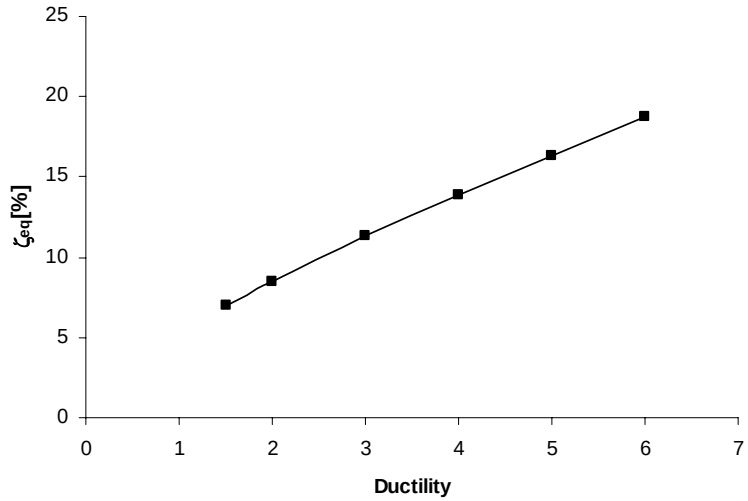


Fig. 4-59 Type 1 | Ring-spring (*R* = 1/3, *r* = 0.1): Equivalent damping versus ductility

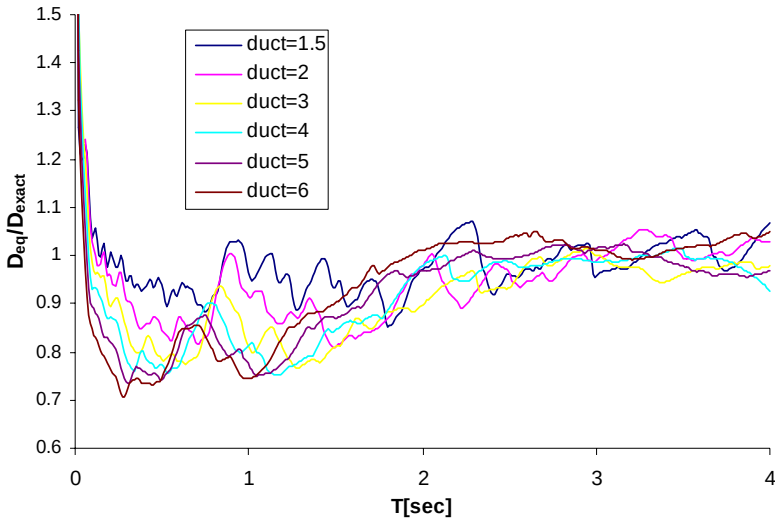


Fig. 4-60 Type 1 | Ring-spring ($R$ = 1/3, $r$ = 0.1): Design to exact displacement (all $\mu$)

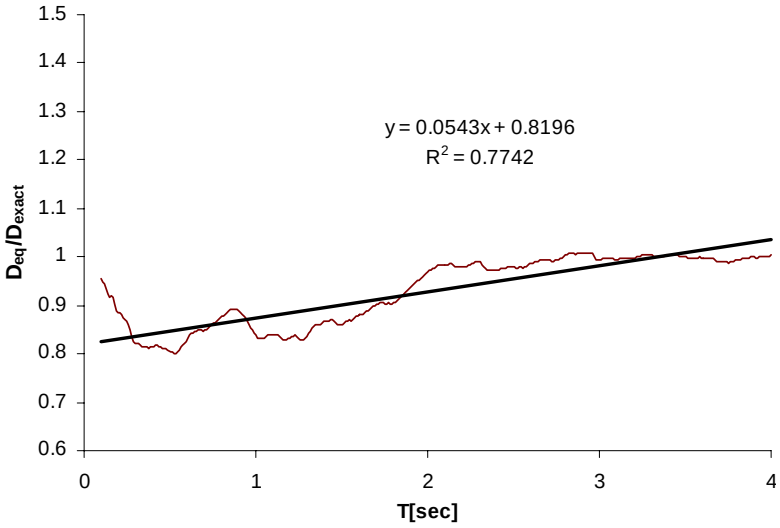


Fig. 4-61 Type 1 | Ring-spring ($R$ = 1/3, $r$ = 0.1): Design to exact displacement (average $\mu$)

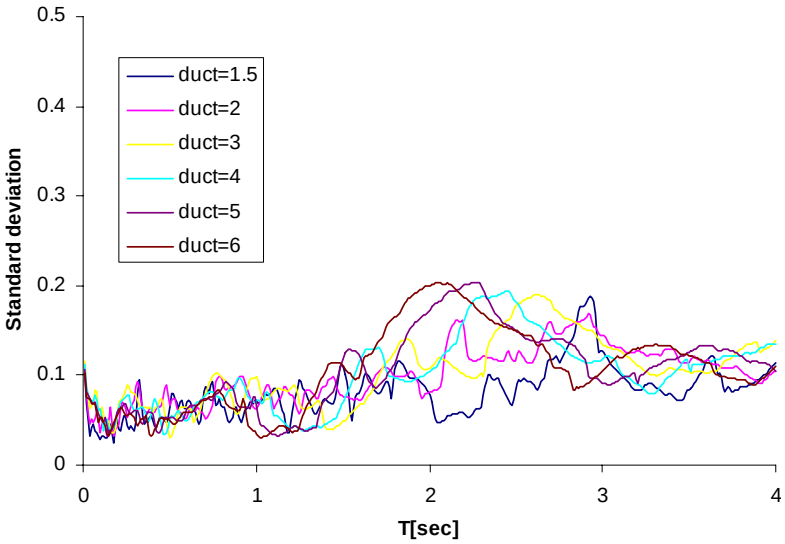


Fig. 4-62 Type 1 | Ring-spring ($R$ = 1/3, $r$ = 0.1): Standard deviation

### Type 2 compatible spectrum | (*R* = 1/3, *r* = 0.1)

Fig. 4-63 through Fig. 4-70 show the steps and the results of the procedure for determining the equivalent period and damping for the ring-spring hysteretic model with $R$ = 1/3 and $r$ = 0.1 (resulting in $r_{low}$ = 0.00357), considering Type 2 compatible spectrum. The equations for equivalent period and damping are expressed as:

$$T_{eq} = T_0 \left[ 1 + 0.244 \left( \mu - 1 \right)^{0.689} \right] \tag{4.28}$$

$$\xi_{eq} = \xi_0 + 4.46 \left( \mu - 1 \right)^{0.638} \quad [\%] \tag{4.29}$$

The expression for determining the maximum vibration period of the SDOF oscillator for which the procedure is applicable is:

$$T_{0\max} = 4.5\, \mu^{-0.31} \leq 4.0 \quad [\text{sec}] \tag{4.30}$$

The procedure generally underestimates the exact displacement up to period values of approximately 1.4 s, and overestimates the exact displacement above this period.

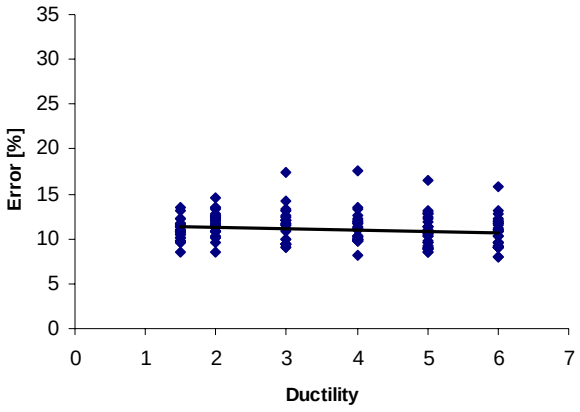


Fig. 4-63 Type 2 | Ring-spring (*R* = 1/3, *r* = 0.1): Average error

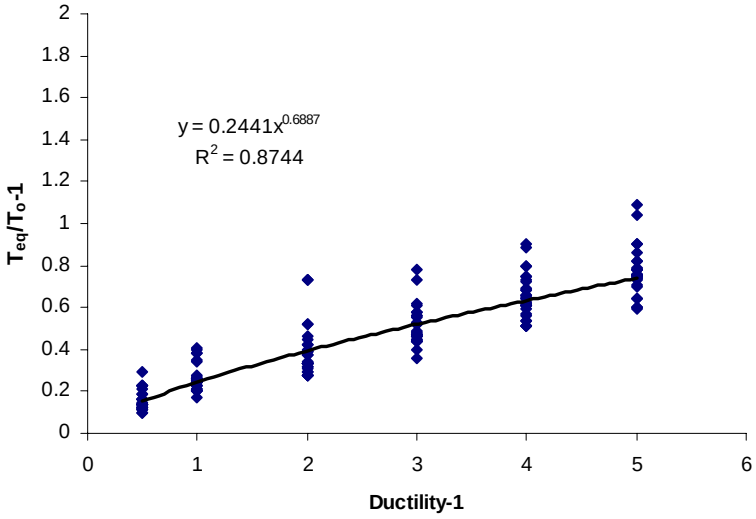


Fig. 4-64 Type 2 | Ring-spring (*R* = 1/3, *r* = 0.1): Period shift versus ductility

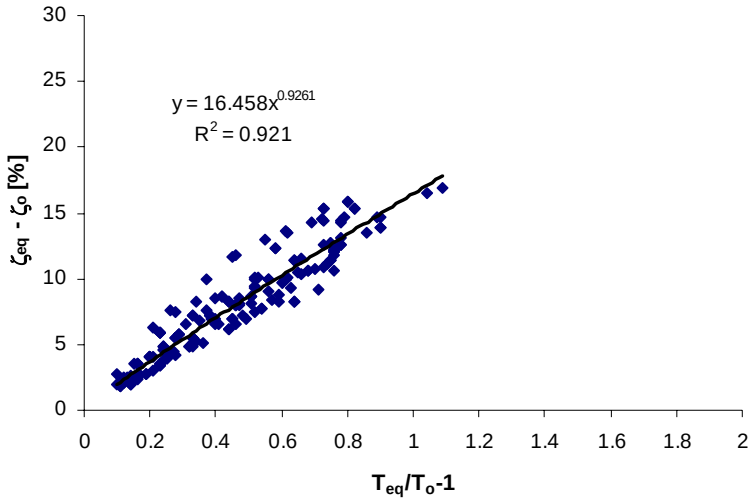


Fig. 4-65 Type 2 | Ring-spring (*R* = 1/3, *r* = 0.1): Equivalent damping versus period shift

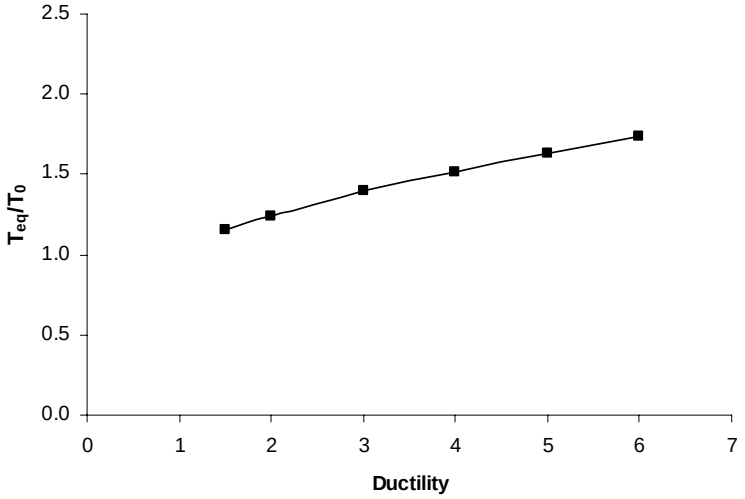


Fig. 4-66 Type 2 | Ring-spring (*R* = 1/3, *r* = 0.1): Equivalent period versus ductility

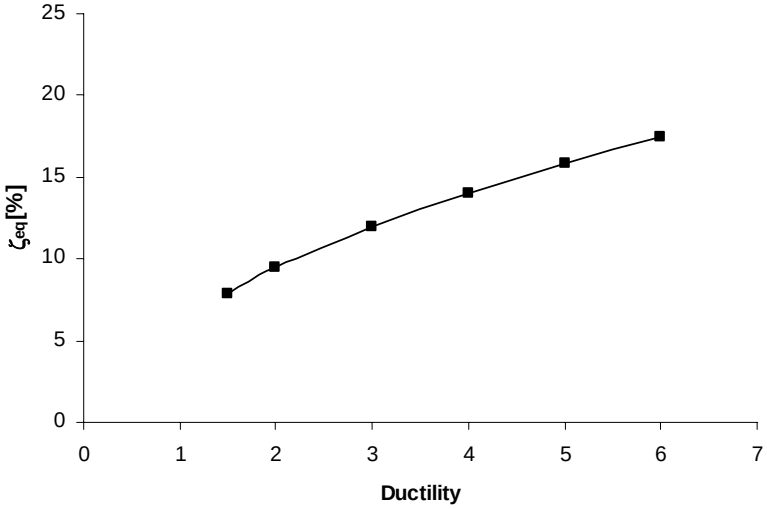


Fig. 4-67 Type 2 | Ring-spring (*R* = 1/3, *r* = 0.1): Equivalent damping versus ductility

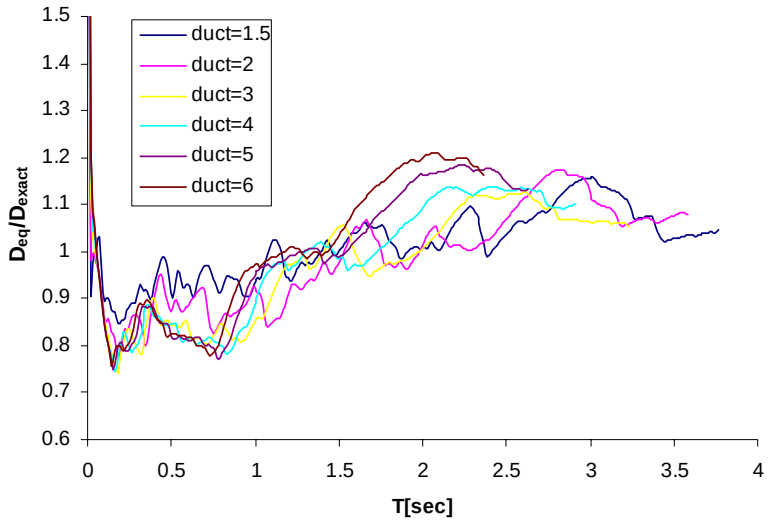


Fig. 4-68 Type 2 | Ring-spring ($R$ = 1/3, $r$ = 0.1): Design to exact displacement (all $\mu$)

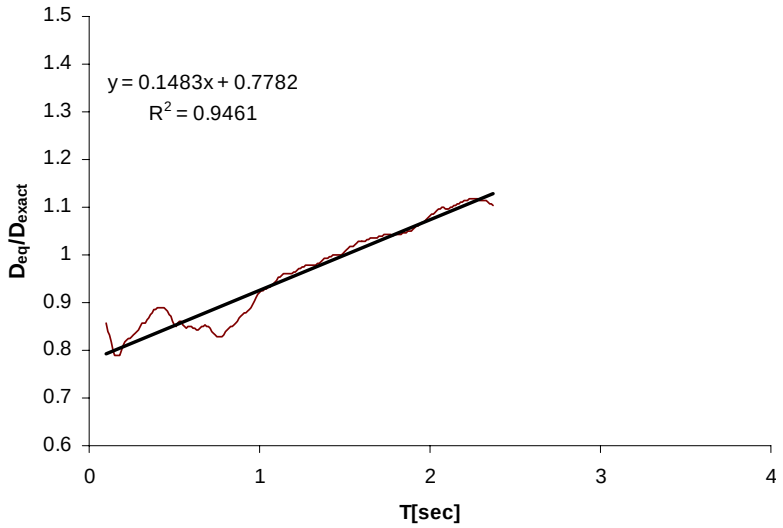


Fig. 4-69 Type 2 | Ring-spring ($R$ = 1/3, $r$ = 0.1): Design to exact displacement (average $\mu$)

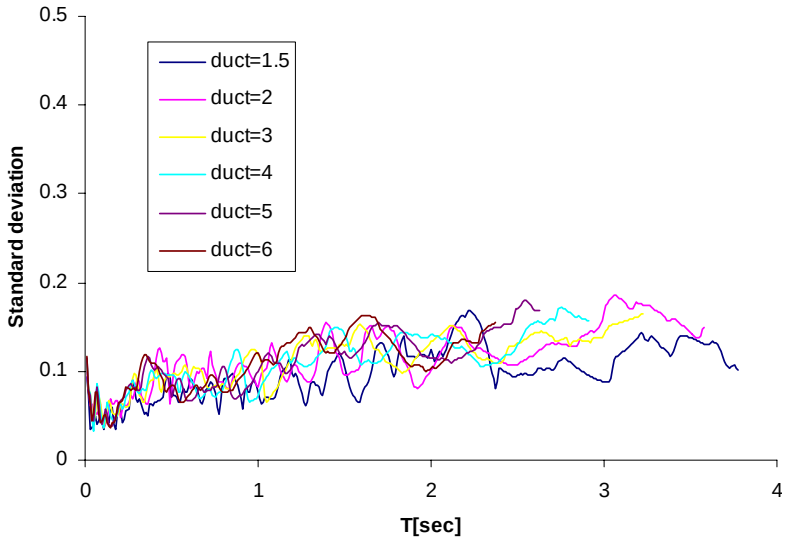


Fig. 4-70 Type 2 | Ring-spring ($R$ = 1/3, $r$ = 0.1): Standard deviation

### Type 1 compatible spectrum | (*R* = 2/3, *r* = 0.05)

Fig. 4-71 through Fig. 4-78 show the steps and the results of the procedure for determining the equivalent period and damping for the ring-spring hysteretic model with *R* = 2/3 and *r* = 0.05 (resulting in $r_{low}$ = 0.00339), considering a Type 1 compatible spectrum. The equations for equivalent period and damping are expressed as:

$$T_{eq} = T_0 \left[ 1 + 0.147 \left( \mu - 1 \right)^{1.09} \right] \tag{4.31}$$

$$\xi_{eq} = \xi_0 + 2.88 \left( \mu - 1 \right)^{0.847} \quad [\%] \tag{4.32}$$

The procedure generally underestimates the exact displacement up to period values of approximately 2 s.

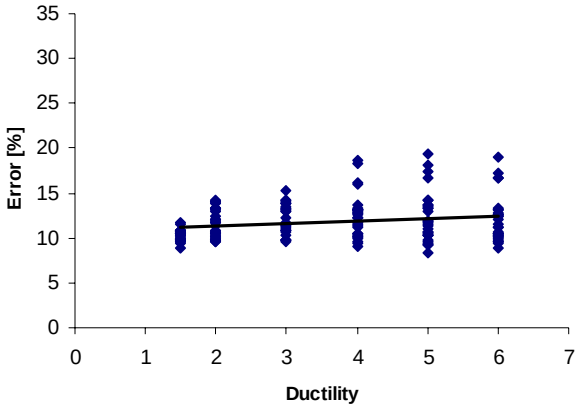


Fig. 4-71 Type 1 | Ring-spring (*R* = 2/3, *r* = 0.05): Average error

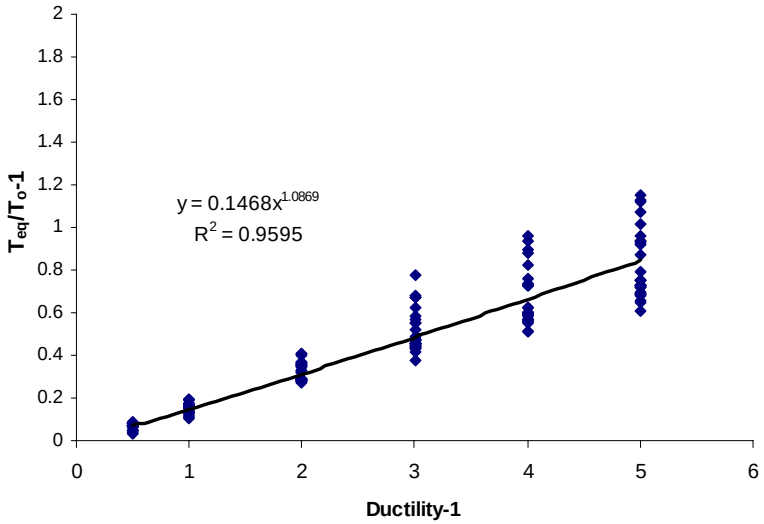


Fig. 4-72 Type 1 | Ring-spring (*R* = 2/3, *r* = 0.05): Period shift versus ductility

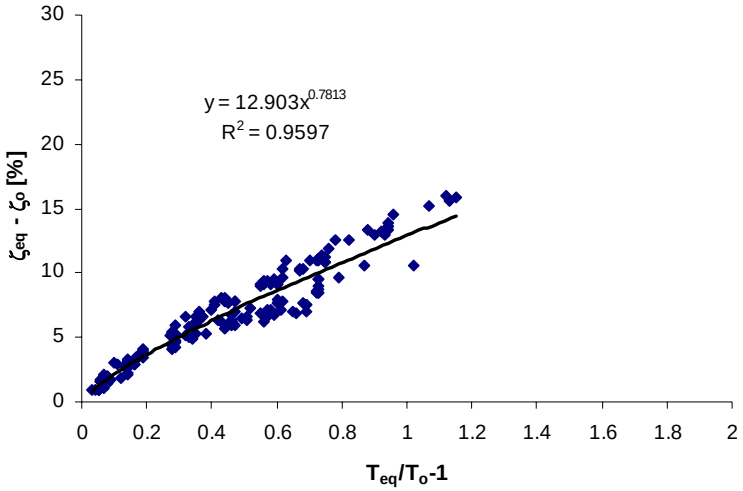


Fig. 4-73 Type 1 | Ring-spring (*R* = 2/3, *r* = 0.05): Equivalent damping versus period shift

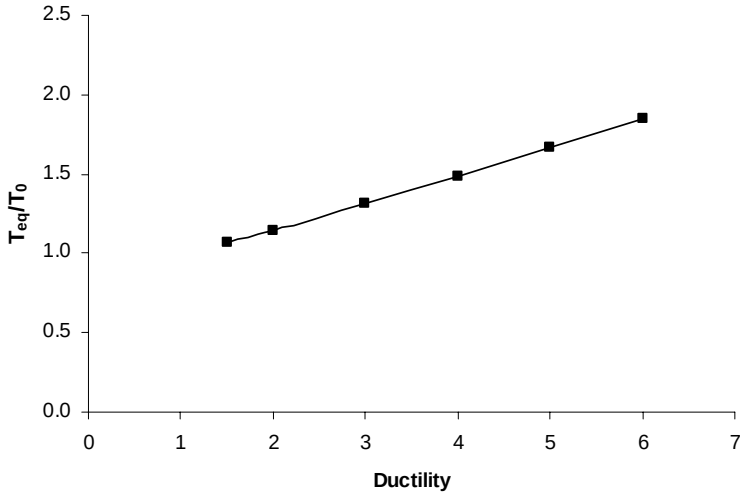


Fig. 4-74 Type 1 | Ring-spring (*R* = 2/3, *r* = 0.05): Equivalent period versus ductility

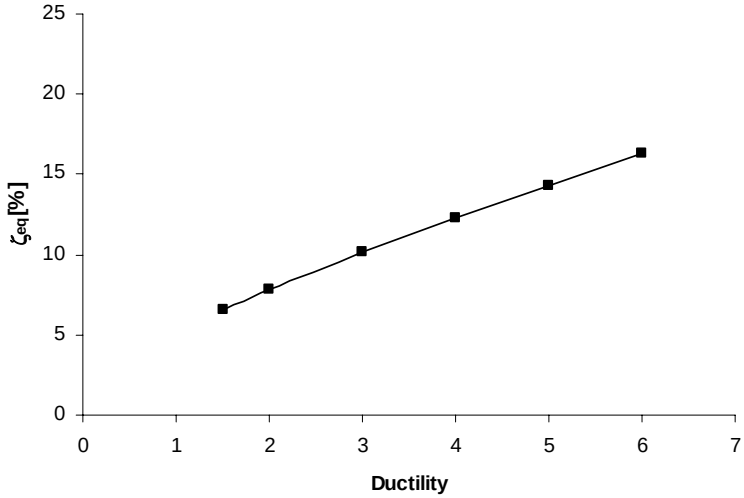


Fig. 4-75 Type 1 | Ring-spring (*R* = 2/3, *r* = 0.05): Equivalent damping versus ductility

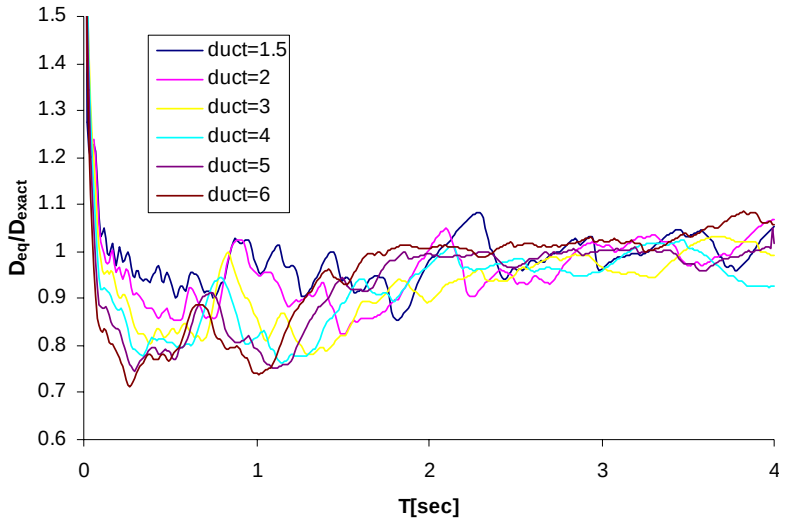


Fig. 4-76 Type 1 | Ring-spring ($R$ = 2/3, $r$ = 0.05): Design to exact displacement (all $\mu$)

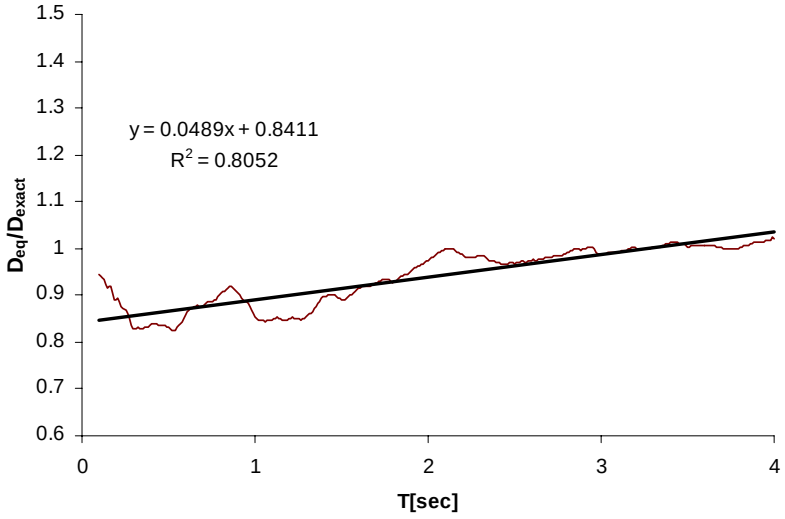


Fig. 4-77 Type 1 | Ring-spring ($R$ = 2/3, $r$ = 0.05): Design to exact displacement (average $\mu$)

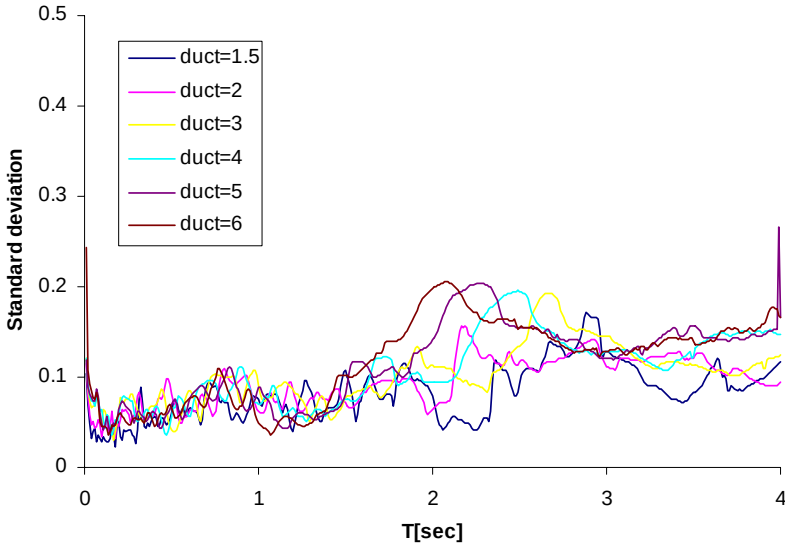


Fig. 4-78 Type 1 | Ring-spring ($R$ = 2/3, $r$ = 0.05): Standard deviation

### Type 2 compatible spectrum | (*R* = 2/3, *r* = 0.05)

Fig. 4-79 through Fig. 4-86 show the steps and the results of the procedure for determining the equivalent period and damping for the ring-spring hysteretic model with *R* = 2/3 and *r* = 0.05 (resulting in $r_{low}$ = 0.00339), considering a Type 2 compatible spectrum. The equations for equivalent period and damping are expressed as:

$$T_{eq} = T_0 \left[ 1 + 0.244 \left( \mu - 1 \right)^{0.720} \right] \tag{4.33}$$

$$\xi_{eq} = \xi_0 + 3.61 \left( \mu - 1 \right)^{0.640} \quad [\%] \tag{4.34}$$

The expression for determining the maximum vibration period of the SDOF oscillator for which the procedure is applicable is:

$$T_{0\max} = 4.5\, \mu^{-0.31} \leq 4.0 \quad [\text{sec}] \tag{4.35}$$

The procedure underestimates the exact displacement up to period values of approximately 1.4 s, and overestimates the exact displacement above this period.

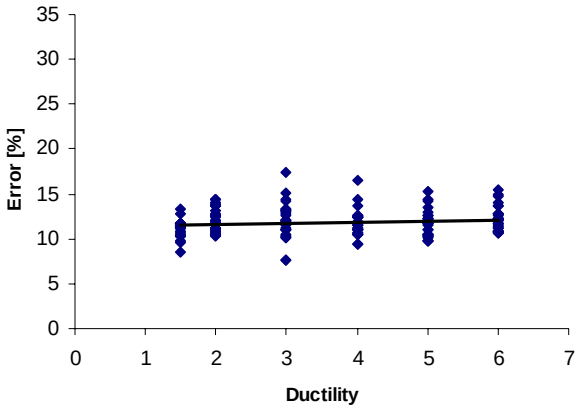


Fig. 4-79 Type 2 | Ring-spring (*R* = 2/3, *r* = 0.05): Average error

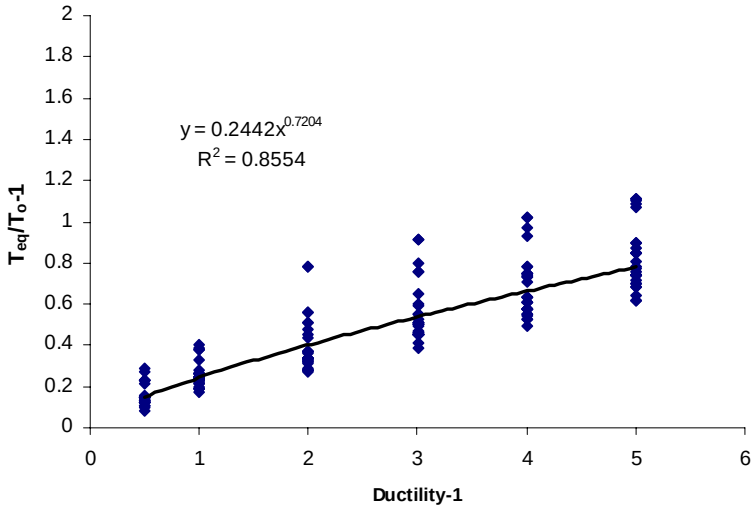


Fig. 4-80 Type 2 | Ring-spring (*R* = 2/3, *r* = 0.05): Period shift versus ductility

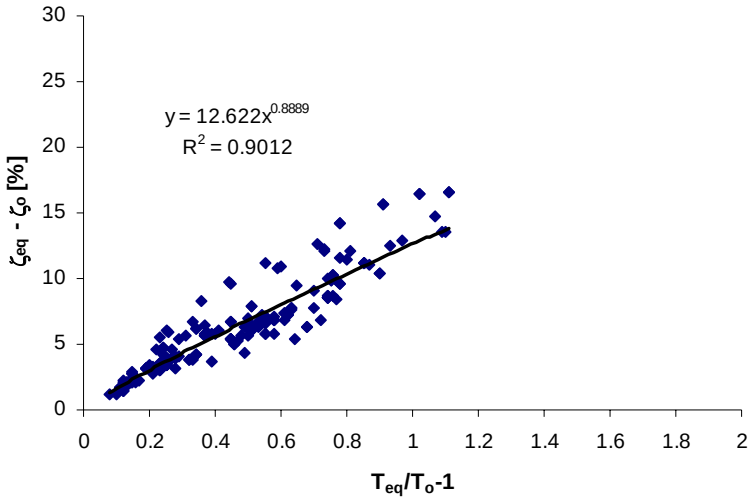


Fig. 4-81 Type 2 | Ring-spring (*R* = 2/3, *r* = 0.05): Equivalent damping versus period shift

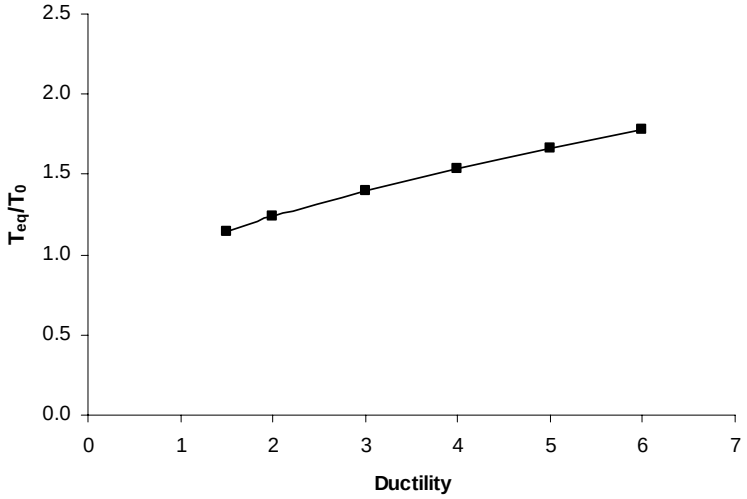


Fig. 4-82 Type 2 | Ring-spring (*R* = 2/3, *r* = 0.05): Equivalent period versus ductility

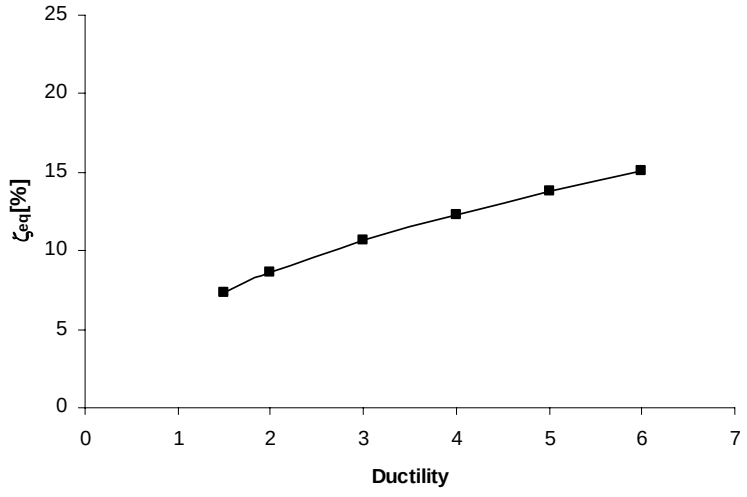


Fig. 4-83 Type 2 | Ring-spring (*R* = 2/3, *r* = 0.05): Equivalent damping versus ductility

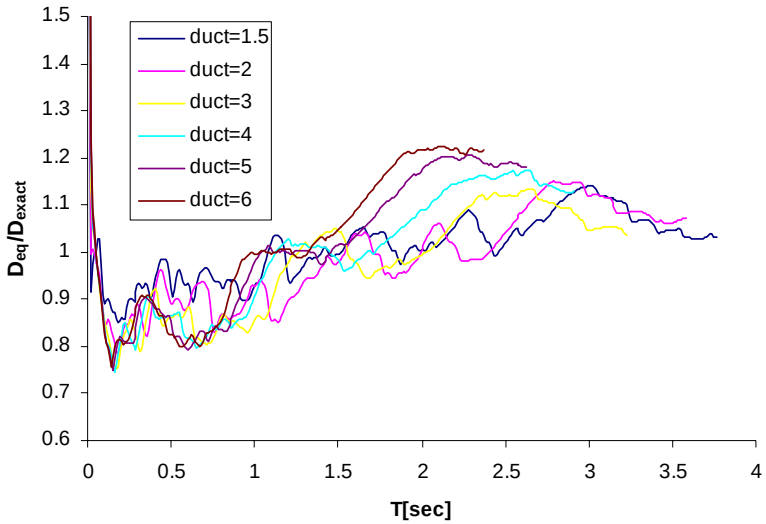


Fig. 4-84 Type 2 | Ring-spring ($R$ = 2/3, $r$ = 0.05): Design to exact displacement (all $\mu$)

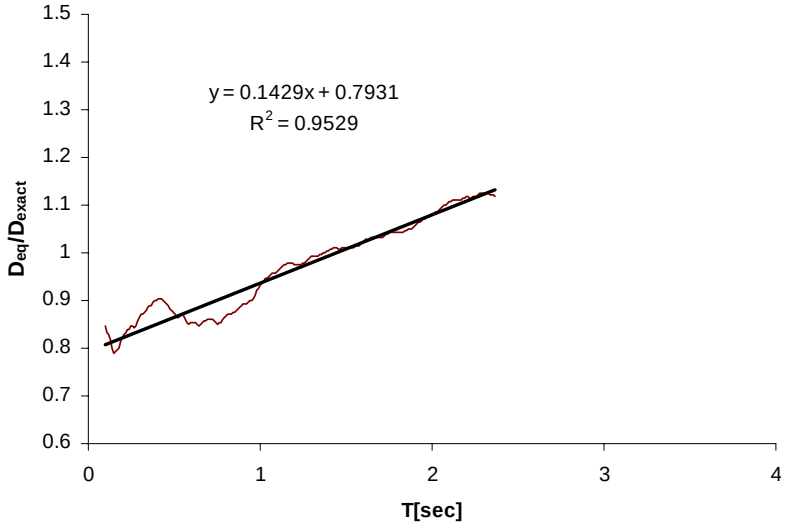


Fig. 4-85 Type 2 Ring-spring ($R$ = 2/3, $r$ = 0.05): Design to exact displacement (average $\mu$)

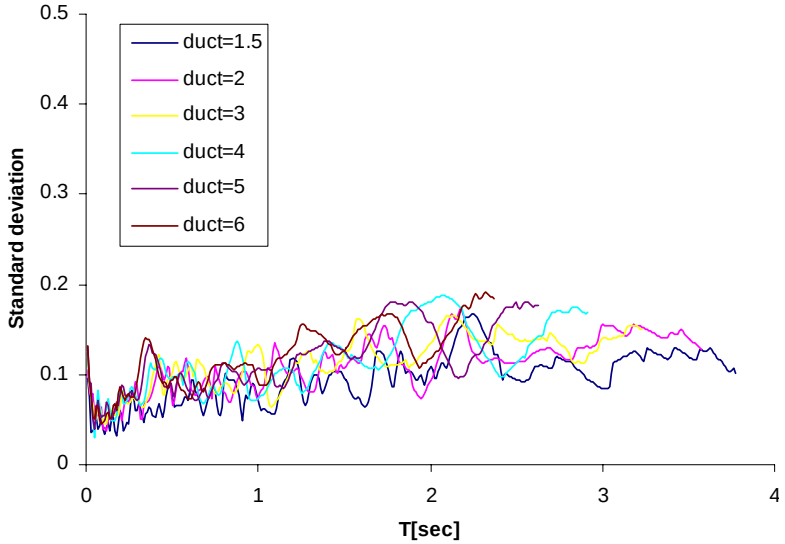


Fig. 4-86 Type 2 | Ring-spring ($R$ = 2/3, $r$ = 0.05): Standard deviation

## 4.3 Discussion of the Results

The resulting equations for computing equivalent damping and periods can be introduced in the following form:

$$T_{eq} = T_0 \left[ 1 + A\left(\mu - 1\right)^a \right] \tag{4.36}$$

$$\xi_{eq} = \xi_0 + B\left(\mu - 1\right)^b \quad [\%] \tag{4.37}$$

in which the coefficients *A*, *a*, *B* and *b* are given in Table 4-2, for each hysteretic model and corresponding set of parameters for Type 1 and 2 response spectra.

Table 4-2 Coefficients for hysteretic models equivalent parameters equations

| Hysteretic Model | Spectra Type | Equation (4.36) | | Equation (4.37) | | at $\mu$ = 6 | |
|---|---|---|---|---|---|---|---|
| | | *A* | *a* | *B* | *b* | $T_{eq}/T_0$ | $\xi_{eq}$-$\xi_0$ (%) |
| **Bilinear kinematic** | 1 | 0.153 | 1.02 | 2.14 | 1.02 | 1.79 | 11.0 |
| | 2 | 0.252 | 0.719 | 3.35 | 0.873 | 1.80 | 13.7 |
| **Ring Spring** | 1 | 0.159 | 1.10 | 3.66 | 0.839 | 1.94 | 14.1 |
| *R* =1/3 ; *r* =0.025 | 2 | 0.259 | 0.748 | 4.53 | 0.657 | 1.86 | 13.0 |
| **Ring Spring** | 1 | 0.153 | 1.10 | 3.63 | 0.842 | 1.90 | 14.1 |
| *R* =1/3 ; *r* =0.050 | 2 | 0.255 | 0.726 | 4.52 | 0.650 | 1.82 | 12.9 |
| **Ring Spring** | 1 | 0.143 | 1.07 | 3.52 | 0.845 | 1.81 | 13.7 |
| *R* =1/3 ; *r* =0.100 | 2 | 0.244 | 0.688 | 4.46 | 0.638 | 1.74 | 12.5 |
| **Ring Spring** | 1 | 0.147 | 1.09 | 2.88 | 0.847 | 1.85 | 11.3 |
| *R* =2/3; *r* =0.050 | 2 | 0.244 | 0.720 | 3.61 | 0.640 | 1.78 | 10.1 |

In Table 4-2 are also given the period shift and equivalent damping obtained for a ductility of 6, resulting in period shifts ranging between 1.7 and 1.9, and equivalent damping ratios ranging between 10% and 14% (the lowest values of damping are obtained for the ring-spring model with *R* equal 2/3), with slightly higher values, for the ring-spring model, for the Type 1 spectra.

By examining the parameters of Equations (4.36), it is possible to see that they vary consistently with the Type of spectra, suggesting that, for the ring-spring models, an average value of *A* equal to 0.15 and 0.25, and *a* equal to 1.09 and 0.72, may be defined for the Type 1 and Type 2 spectra, respectively.

Concerning the parameters of Equation (4.37), some variation is observed not only between the type of spectra, but also among the various models, especially between the ring-spring models with *R* equal 1/3 and 2/3. For the two models that consider *R* equal to 1/3, an average value of *B* equal to 3.60 and 4.50, and *b* equal to 0.84 and 0.65, for the Type 1 and Type 2 spectra, respectively, may be defined, irrespective of the considered values of *r*.

The coefficients given in Table 4-2 also show that there are not large differences between the equivalent properties of the bilinear kinematic model and those of the ring-spring model, in spite of the larger damping developed by the bilinear model when subjected to cyclic harmonic displacements. The difference may be due to the fact that under small cycle reversals at ductilities larger than 1, the ring-spring model dissipates considerable amounts of energy with respect to the bilinear model, which needs to complete a full cycle equal to twice the yield displacement, starting from the plateau of the envelope, to overcome the stored elastic energy and start dissipating energy again. This shows the importance of determining equivalent properties based on a particular hysteretic model and on a specific family of earthquakes.

The maximum vibration period of the SDOF oscillator for which the procedure is applicable for Type 2 compatible spectra is limited by the following equation, which may be used for all hysteretic models and spectra Types:

$$T_{0\max} = 4.5\,\mu^{-0.32} \leq 4.0 \quad \text{[sec]} \tag{4.38}$$

Equation (4.38) is plotted on Fig. 4-87, showing that for large ductility values, $T_{0max}$ approximates to 2.5 seconds.

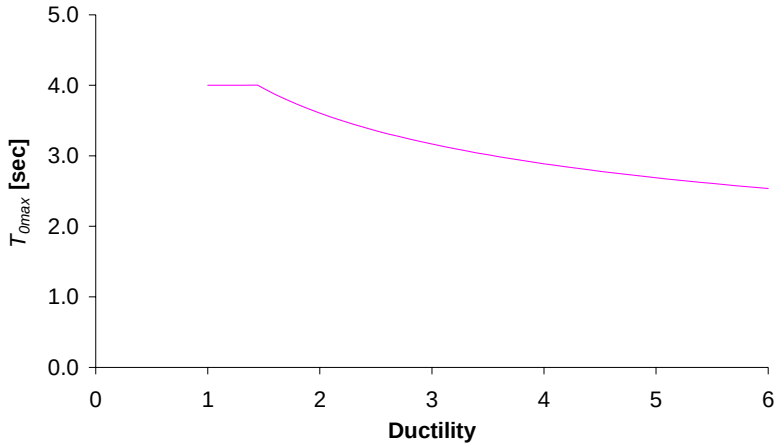


Fig. 4-87 $T_{0max}$ as function of ductility for Type 2 spectra

With regards to the ratio between the predicted displacement and the exact displacement, it is possible to observe that for all cases studied, the deviation of the ratio $D_{eq}/D_{exact}$ with respect to 1 increases with the increase of ductility, which for the case of the ring-spring model reaches minimum values of 0.70, in the low period range, and maximum values of 1.25, in the high period range.

In general, the standard deviation of $D_{eq}/D_{exact}$ increases with the increase of period and ductility, up to a maximum value of 0.2 for the ring-spring models (a higher value, equal to 0.45, is obtained for the kinematic model).

Considering the average of all ductilities for the ring-spring models, it is possible to express the ratio $D_{eq}/D_{exact}$ as a function of the initial period $T_0$ for the two Types of spectra:

$$\frac{D_{eq}}{D_{exact}} = 0.0546\,T_0 + 0.823 \quad \text{[sec]} \qquad \text{Type 1 spectra} \tag{4.39}$$

$$\frac{D_{eq}}{D_{exact}} = 0.152\,T_0 + 0.778 \quad \text{[sec]} \qquad \text{Type 2 spectra} \tag{4.40}$$

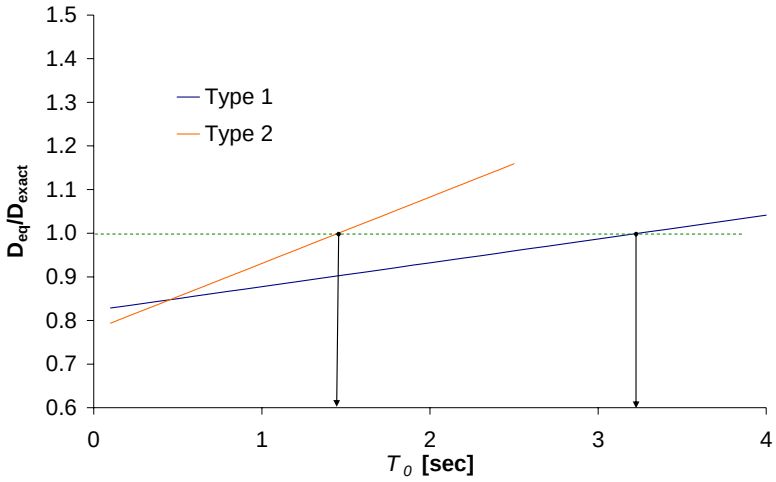


Fig. 4-88 $D_{eq}/D_{exact}$ as function of $T_0$ for Type 1 and Type 2 spectra, average of all ductilities

Equations (4.39) and (4.40) are plotted in Fig. 4-88, showing that $D_{eq}/D_{exact}$ equals to 1 for period values of 3.23 and 1.48 seconds for the Type 1 and Type 2 spectra, respectively.

In order to better assess the results obtained from the analysis, the equivalent period and damping obtained from the analysis for the ring-spring models are compared with the corresponding values obtained at peak displacement with reference to the secant stiffness and energy dissipated by cycles of harmonic displacement (Blandon, 2004). For this, the secant stiffness and energy dissipated as a function of ductility are defined referring to the parameters of Fig. 3-5:

$$K_{\sec} = \frac{F_y + r K_0 d_y (\mu - 1)}{\mu d_y} \tag{4.41}$$

$$\xi_{harmonic} = \frac{1}{\pi} \frac{(A_1 + A_2) - (A_3 + A_4)}{2\mu\left[1 + r(\mu - 1)\right]}$$

$$A_1 + A_2 = (R+1)(1-R) + \left[2 + r(\mu - 1)\right](\mu - 1)$$

$$A_3 + A_4 = R^2\left[2 + r_{lower}(\beta - 1)\right](\beta - 1) + \left[(R+1) + r_{lower} R(\beta - 1) + r(\mu - 1)\right](\mu - \beta R) \tag{4.42}$$

$$\beta = \frac{(1-R) + r(\mu - 1) + R\, r_{lower} - r_{steep}\,\mu}{R\left(r_{lower} - r_{steep}\right)}$$

The equivalent values of period and damping, $T_{eq}^{*}$ and $\xi_{eq}^{*}$, computed from Equations (4.41) and (4.42), are expressed as:

$$T_{eq}^{*} = T_0 \sqrt{\frac{\mu}{1 + r(\mu - 1)}} \tag{4.43}$$

$$\xi_{eq}^{*} = \xi_0 + 100\,\xi_{harmonic} \quad [\%] \tag{4.44}$$

At each level of ductility $\mu$, it is possible to find a value $\lambda$, which multiplies the ductility of equations (4.41) through (4.44), such that the equivalent period of Equations (4.36) and (4.43), and the equivalent damping of Equations (4.37) and (4.44), are equal:

$$T_{eq}(\mu) \doteq T_{eq}^{*}(\lambda\mu) \tag{4.45}$$

$$\xi_{eq}(\mu) \doteq \xi_{eq}^{*}(\lambda\mu) \tag{4.46}$$

Since the same value of λ is used in Equations (4.45) and (4.46), an optimization procedure is carried out by minimizing at each ductility level the error $\varepsilon(\lambda,\mu)$ that results from the difference between Equations (4.36) and (4.43), and Equations (4.37) and (4.44):

$$\varepsilon(\lambda,\mu) = \left\{ \left[ \frac{T_{eq}^{*} - T_{eq}}{T_{eq}} \right]^2 + \left[ \frac{\xi_{eq}^{*} - \xi_{eq}}{\xi_{eq}} \right]^2 \right\}^{1/2} \tag{4.47}$$

The variation of λ as a function of ductility is shown in Fig. 4-89 for the particular case of the ring-spring model with $R$ = 1/3 and $r$ = 0.025, varying from 1, for a ductility of 1, to a minimum of 0.47 for a ductility of 4, and then increasing again. The dependency of λ with respect to ductility may be approximated with a polynomial function expressed by the following equation:

$$\lambda = \frac{1}{\mu^{\beta}} + \alpha(\mu - 1) \tag{4.48}$$

where $\beta$ and $\alpha$ are obtained by minimising the overall error of Equation (4.47) for ductility values comprised between 1 and 6. Equation (4.48) is shown in Fig. 4-89, for $\beta$ and $\alpha$ equal to 0.85 and 0.060, respectively, derived for the ring-spring model with $R$ = 1/3 and $r$ = 0.025.

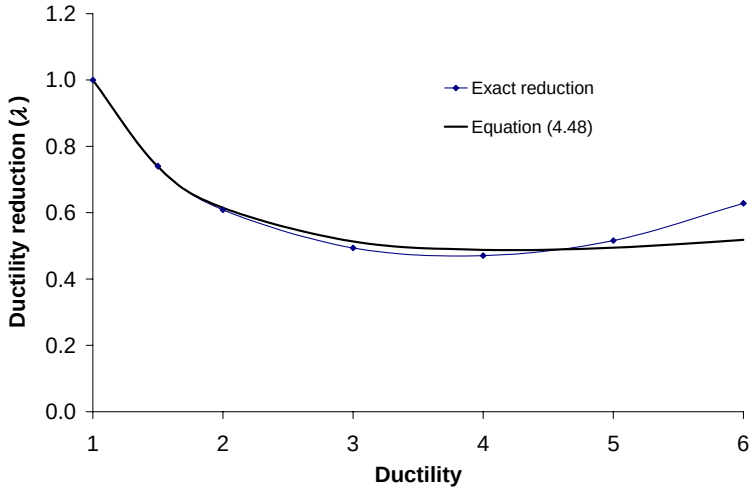


Fig. 4-89 Ductility reduction ($\lambda$) as a function of ductility for the ring-spring model with $R$ = 1/3 and $r$ = 0.025

The comparison between the expressions given by Equation (4.36), and Equation (4.43) with $\lambda$ equal to 1 (equivalent period computed from secant stiffness at ductility $\mu$) and $\lambda$ obtained from Equation (4.48) (equivalent period computed from secant stiffness at ductility $\lambda\mu$), is shown in Fig. 4-90.

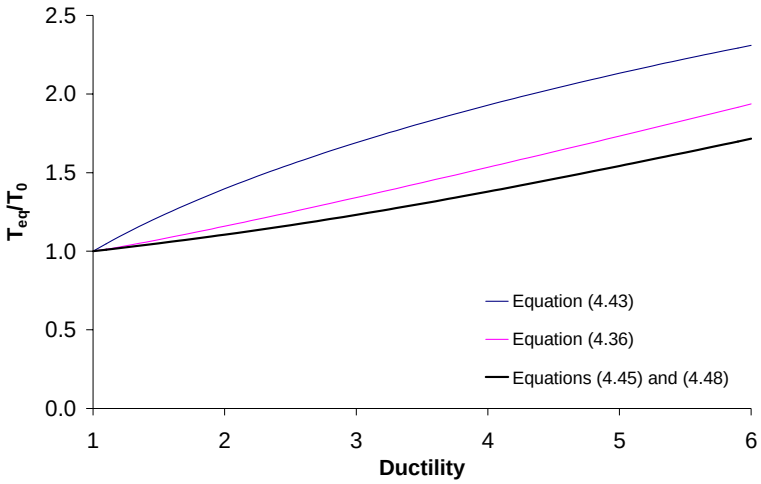


Fig. 4-90 Comparison between different expression to compute $T_{eq}$ for the ring-spring model with $R$ = 1/3 and $r$ = 0.025

Similarly, the comparison between the expressions given by Equation (4.37), and Equation (4.44) with $\lambda$ equal to 1 (equivalent damping computed from harmonic displacements cycling about $\mu$) and $\lambda$ obtained from Equation (4.48) (equivalent damping computed from harmonic displacements cycling about ductility $\lambda\mu$), is shown in Fig. 4-91.

Fig. 4-89 and Fig. 4-90 show that the correlation between Equations (4.36) and (4.37), with Equations (4.43) and (4.44), using the $\lambda$ factor from Equation (4.48), is better for the equivalent damping than for the equivalent period.

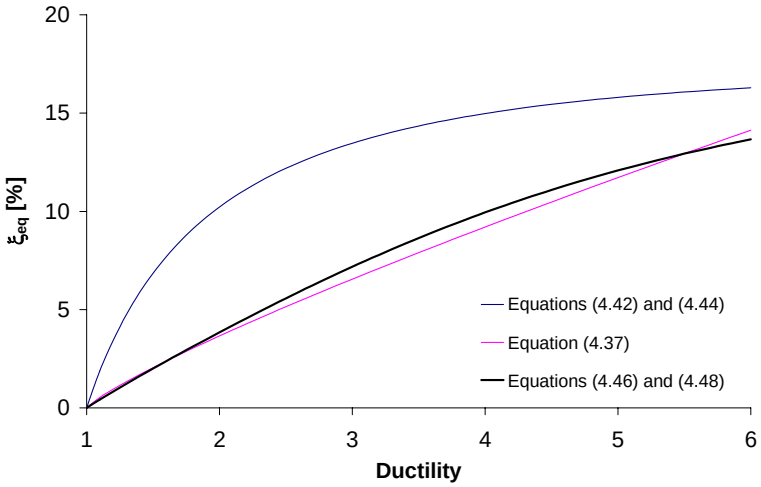


Fig. 4-91 Comparison between different expression to compute $\xi_{eq}$ for the ring-spring model with $R$ = 1/3 and $r$ = 0.025

The values of $\beta$ and $\alpha$ are calculated for the remaining ring-spring models and are summarised in Table 4-3, from where it is possible to define, for $R$ = 1/3, $\beta$ and $\alpha$ values of 0.85 and 0.064, and 0.63 and 0.030, for the Type 1 and Type 2 spectra, respectively. For $R$ = 2/3 Equation (4.43), together with the reduction of the ductility by factor $\lambda$ from Equation (4.48), underestimates the equivalent damping given by Equation (4.37) for ductility values above 3.

Table 4-3 $\beta$ and $\alpha$ coefficients of Equation (4.48) for computing the ductility reduction factor $\lambda$.

| Hysteretic Model | Spectra Type | Equation (4.48) | |
|---|---|---|---|
| | | $\beta$ | $\alpha$ |
| **Ring Spring** | 1 | 0.85 | 0.060 |
| $R$ =1/3 ; $r$ =0.025 | 2 | 0.65 | 0.028 |
| **Ring Spring** | 1 | 0.85 | 0.063 |
| $R$ =1/3 ; $r$ =0.050 | 2 | 0.65 | 0.033 |
| **Ring Spring** | 1 | 0.85 | 0.068 |
| $R$ =1/3 ; $r$ =0.100 | 2 | 0.60 | 0.028 |
| **Ring Spring** | 1 | 0.70 | 0.108 |
| $R$ =2/3; $r$ =0.050 | 2 | 0.35 | 0.041 |

Concerning the parameters corresponding to the ductility reduction to be applied to the bilinear kinematic model, it is expected that they should reflect a larger reduction than that obtained for the ring-spring model, reflecting the larger damping dissipated by the bilinear model under cyclic harmonic displacements.

# 5 Recommendations

From the work carried out in the present report the following recommendations are proposed to improve the error minimization process, the type of expressions used and a scheme for defining equivalent properties based on a reduction of the ductility.

## 5.1 Error minimization

The error minimization from Equation (4.7) for computing the optimal pair ($\xi_{eq}$,$T_{eq}$) is performed across all *N* periods for each of the *K* earthquakes and at each of the *J* ductility levels considered in the analysis, resulting into *KxJ* optimum pairs of values. From these values, the best fit is found as shown in Fig. 4-8 and Fig. 4-9, with expressions of the type shown in Equation (4.8) and (4.9), between $T_{eq}/T_0$-1 and $\mu$-*1*, and between $\xi_{eq}$-$\xi_0$ and $T_{eq}/T_0$-1.

This procedure, adopted in the present report, is different from the methodology proposed by Iwan (1980), where the best fit is found from only *J* optimum pairs of values, resulting from an error minimization performed across all periods and earthquakes at each level of ductility (more precisely, the number of optimum pairs equals *J* times the number of hysteretic models considered in the analysis).

It is recommended to adopt an error minimization procedure similar to that proposed by Iwan, as it is more consistent to perform the error minimization through all earthquakes, rather than for each single earthquake, and then perform the best fit with the optimum values at each ductility level.

Nevertheless, one modifications from Iwan's approach is proposed: not to consider more than one hysteretic model when computing the best fit formula, as it is presumed that each hysteretic model will have its particular equivalent parameters. Moreover, the analysis should be performed for a series of earthquakes of similar characteristics (near or far field; medium or large intensity, etc.), since for each category of earthquakes different parameters may result for describing equivalent properties, as demonstrated in the present report.

Summarizing, the error minimization should be made for all *N* periods and *K* earthquakes for each ductility *j* according to the following expressions:

$$\varepsilon_{ik}(\xi_{eq},T_{eq}/T_0)=\frac{SD_{eq}\left(EQ_k,T_i,(T_{eq}/T_0),\xi_{eq}\right)}{SD_n\left(EQ_k,\mu_j,T_i,\xi_0\right)}-1 \tag{5.1}$$

$$\bar{\varepsilon}_j(\xi_{eq},T_{eq}/T_0)=\frac{1}{K}\sum_{k=1}^{K}\left[\sum_{i=1}^{N}\frac{\varepsilon_{ik}}{N}\right] \tag{5.2}$$

where $SD_{eq}$ is the maximum displacement obtained from linear time history analysis for earthquake $EQ_k$ considering a linear model with equivalent properties $\xi_{eq}$ and $T_{eq}/T_0$, with $T_0$ equal to $T_i$; and $SD_n$ is the exact displacement obtained from nonlinear time history analysis for the same earthquake $EQ_k$, considering a particular hysteretic model at ductility ratio $\mu_j$, initial stiffness $T_0$ equal to $T_i$, and viscous damping $\xi_0$.

The optimal pair ($\xi_{eq}$,$T_{eq}/T_0$) at ductility $\mu_j$ is that for which the minimum average error $\bar{\varepsilon}_j$ is obtained.

In order to verify that the solution is unique, plots of the contours of the averaged errors corresponding to the pairs of $\xi_{eq}$ and $T_{eq}/T_o$ considered in the analysis should be made for each of the ductility levels considered. In addition, the standard deviation of the error should

also be plotted in a similar graph, in order to measure the spread of variation of the error for each pair of equivalent properties, according to the following expression:

$$SDV\left[\varepsilon_j(\xi_{eq,}T_{eq}/T_0)\right]=\sqrt{\frac{\sum_{k=1}^{K}\sum_{i=1}^{N}\left(\varepsilon_{ik}-\overline{\varepsilon}_j\right)^2}{(KN-1)}} \tag{5.3}$$

The remaining steps for determining the relationships for period shift and equivalent damping as a function of ductility are the same as those proposed at Step 3 of Section 4.2.1 (Equations (4.8) through (4.10)).

It is recommended to derive these equations with the procedure proposed herein and compare the results with those obtained in the present report, by computing the ratio of the equivalent solution with respect to the exact one, as shown in Fig. 4-12 through Fig. 4-14.

## 5.2 Type of expressions

In general, the equivalent damping of nonlinear systems tends to asymptote at large levels of ductility, which is best described by a relationship of the type:

$$\xi_{eq}-\xi_0=B^*\left(1-\frac{1}{\mu^{b^*}}\right) \tag{5.4}$$

rather than by an equation of the type as (4.10), where the equivalent damping increases with ductility without tending to an asymptote. For this reason it is proposed to find the expressions to compute the equivalent properties as follows:

1. Perform the error minimization as described in Section 5.1, and obtain the pair of optimum ($\xi_{eq}$,$T_{eq}/T_0$) at each ductility level *j*.
2. Plot $T_{eq}/T_0$ as a function of ductility $\mu$ and find the coefficient *a** that best fits the numerical results using the following expression:

$$\frac{T_{eq}}{T_0}=\mu^{a^*} \tag{5.5}$$

3. Plot $\xi_{eq}$-$\xi_0$ as a function of period $T_{eq}/T_0$ and find the coefficients *B** and *c* that best fit the numerical results using the following expression:

$$\xi_{eq}-\xi_0=B^*\left[1-\frac{1}{\left(T_{eq}/T_0\right)^c}\right] \tag{5.6}$$

4. By substituting Equation (5.5) into (5.6), the value of *b** is computed as *c*·*a**.
5. By using the expressions from Equations (5.4) and (5.6), compute the ratios between the equivalent and the exact displacement, and the associated standard deviation, for a range of periods $T_0$ and ductilities $\mu$, as shown in Fig. 4-12 through Fig. 4-14, and compare the ability of this procedure, with respect to that proposed in Section 5.1, in predicting the exact displacement.

## 5.3 Ductility reduction

The application of the procedures suggested in Sections 5.1 and 5.2 should lead to a specific set of parameters for the expressions approximating the equivalent damping and period shift for each hysteretic model and category of earthquakes considered. However, following the procedure outlined in Section 4.3, it may be possible to define a reduction factor $\lambda$ of the ductility, that applied in conjunction with the expressions to compute the secant stiffness and hysteretic energy dissipated by harmonic cycles at maximum displacement (e.g., Equations (4.42) and (4.43) for the ring-spring model), may allow to define an expression for determining $\lambda$ as a function of $\mu$ common to a class of hysteretic models (for example, for all ring-spring models, irrespective of the $R$ and $r$ values considered) and category of earthquakes. The proposed procedure is as follows:

1. Perform the error minimization following the procedure suggested in Section 5.1 by varying the value of $\lambda$ from 1 to a value near to 0, so that the values of equivalent damping and period shift at a given ductility level are derived from the secant stiffness and hysteretic energy dissipated by harmonic cycles at the considered ductility reduced by factor $\lambda$. For example, for the ring-spring model the equivalent properties are computed from the following expressions:

$$\frac{T_{eq}}{T_0} = \sqrt{\frac{\lambda\mu}{1 + r\left(\lambda\mu - 1\right)}} \tag{5.7}$$

$$\xi_{eq}^{\ *} = \xi_0 + \xi_{harmonic}(\lambda\mu) \tag{5.8}$$

   $\xi_{harmonic}$ is computed from Equation (4.42) by substituting $\mu$ by $\lambda\mu$. The average error and standard deviation are computed from:

$$\varepsilon_{ik}(\lambda,\xi_0) = \frac{SD_{eq}\left(EQ_k, T_i, \lambda, \xi_0\right)}{SD_n\left(EQ_k, \mu_j, T_i, \xi_0\right)} - 1 \tag{5.9}$$

$$\overline{\varepsilon}_j(\lambda,\xi_0) = \frac{1}{K}\sum_{k=1}^{K}\left[\sum_{i=1}^{N}\frac{\varepsilon_{ik}}{N}\right] \tag{5.10}$$

$$SDV\left[\varepsilon_j(\lambda,\xi_0)\right] = \sqrt{\frac{\sum_{k=1}^{K}\sum_{i=1}^{N}\left(\varepsilon_{ik} - \overline{\varepsilon}_j\right)^2}{\left(KN - 1\right)}} \tag{5.11}$$

2. For each of the considered ductilities $\mu_j$, plot the average error and standard deviation of the error as a function of $\lambda$ and determine the value of $\lambda$ corresponding to the minimum average error and standard deviation.
3. Find the coefficients $\beta$ and $\alpha$ that best approximate Equation (4.48) to the variation of $\lambda$, obtained from the error minimization process, as a function of the considered ductilities.[1]
4. By using the expressions from Equations (5.7) and (5.8), together with Equation (4.48), with $\beta$ and $\alpha$ obtained from the previous step, compute the ratios between the equivalent and the exact displacement, and the associated standard deviation, for a range of periods $T_0$ and ductilities $\mu$, as shown in Fig. 4-12 through Fig. 4-14, and

[1] The variation of $\lambda$ may also be multi-linear, starting from 1 at $\mu$ =1, down to a constant value and then rising up again to 1 and remaining constant for large ductility values.

compare the ability of this procedure to predict the exact displacements with the equivalent properties.

Repeat steps 1 through 4 for different combinations of $R$ and $r$, and compute the corresponding values of $\beta$ and$\alpha$. Plot Equation (4.48) corresponding to each of the considered combinations of $R$ and $r$, and compute an average curve for which a new set of $\beta$ and $\alpha$ coefficients are found. If the difference between the values obtained from Equation (4.48) using the averaged coefficients and the coefficients corresponding to each $R$ and $r$ combination is acceptable, then the averaged coefficients may be used for all ring-spring models, otherwise, a specific set of coefficients must be used for each $R$ and $r$ combination (or possibly for each value of $R$, irrespectively of $r$).

The method of determining equivalent properties using a ductility reduction is advantageous only in the case where a common set of coefficients $\beta$ and $\alpha$ can be used for a class of hysteretic models and family of earthquakes. On the contrary, the advantage of the method is lost if a specific reduction of ductility needs to be defined for each variation of the hysteretic model (i.e., for different values of $R$ and $r$), in that case the methodologies proposed in Sections 5.1 and 5.2 are preferable, since they are simpler to apply and are more compact in form.

Finally, it is recommended to apply this procedure to a bilinear or elastoplasitc model as well, and compare the associated variation of $\lambda$ with that obtained for the ring-spring model, in order to clarify the fact that similar equivalent properties may obtained for the ring-spring and bilinear kinematic models.

# 6 Conclusions

A literature review on the different methodologies proposed to date to derive the equivalent properties of a viscoelastic linear system capable of approximating the maximum earthquake response of a SDOF hysteretic nonlinear system has been presented. The procedure proposed by Iwan and Gates (1979) and Iwan (1980), with modifications on the error minimization and on the number and type of earthquakes, periods considered and hysteretic models, has been adopted in the present report for deriving equivalent viscoelastic properties of two types of hysteretic models.

In particular, equivalent properties of period shift (with respect to the period corresponding to the initial stiffness of the nonlinear model) and viscous damping were derived considering 60 synthetic earthquakes compatible with Type 1 and Type 2 Eurocode 8 response spectra for two classes of hysteretic models: bilinear kinematic and ring-spring.

The results show that for the two hysteretic models considered, the displacements computed from the visocelastic model with equivalent properties approximate well to the displacements computed from the nonlinear model, considering the average of all the earthquakes and ductilities analysed. The ratio between the approximate and the exact displacement ranges between 0.70, in the low period range, and 1.25 for large periods on the order of 3 to 4 seconds. This ratio tends to a value equal to 1 at periods equal to 3.2 and 1.5 seconds for the Type 1 and Type 2 spectra.

The analysis indicates that the coefficients of the equations for determining the equivalent period and damping of the viscoelastic system are dependant on the type of spectra considered, suggesting that any expression proposed for deriving equivalent properties must refer to a particular family of earthquakes (or fault region).

The results also show that in spite of the larger damping dissipated by the bilinear kinematic model when subjected to cyclic harmonic displacements, the equivalent properties of this model are similar to those obtained for the ring-spring model when predicting maximum response to earthquake excitation.

Closed form expressions for determining the secant stiffness and equivalent damping corresponding to the energy dissipated by cycles of harmonic displacement at maximum displacement have been derived for the ring-spring model. An expression for determining a reduction factor of the ductility at maximum displacement has been proposed, such that the equivalent properties determined from the secant stiffness and damping from harmonic displacements approximate the equivalent properties determined from the error minimization process. This reduction varies from 1, at a ductility of 1, to values on the order of 0.50, for ductilities between 4 and 6.

A set of recommendations is proposed on improvements on the error minimization process, on the type of equations used to express the equivalent properties, and on an error minimization procedure to determine an expression for the reduction of ductility at maximum displacement to obtain equivalent properties based on secant stiffness and damping from cyclic harmonic displacements.

# 7 References

ATC32 (2003) “Improved seismic design criteria for California bridges: Provisional Recommendations”, *Applied Technology Council*, Report No. ATC-32, Redwood City, California.

Blandon C. A. (2004) “Equivalent viscous damping for DDBD”, MSc Thesis, *ROSE School*, Pavia, Italy.

Blandon C. A., Priestley M. J. N. (2005) “Equivalent viscous damping equations for direct displacement based design”, *Journal of earthquake Engineering*, Vol. 9, Special Issue 2, pp. 257-278.

Clough R. W, Penzien J. (1993) “Dynamics of Structures”, *McGraw-Hill International Editors*, Civil Engineering Series, ISBN 0-07-113241-4.

Clough RW, “Johnston S. B., Effect of stiffness degradation on earthquake ductility requirements”, *Proceedings of Japan Earthquake Engineering Symposium*, Tokyo, Japan, 1996, 227-231.

Dobry R., Idriss I. M., Ng E. (1978) “Duration characteristics of horizontal components of strong-motion earthquake records”, *Bulletin of the Seismological Society of America*, Vol. 68, No. 5, pp. 1487-1520, October.

Eurocode 8 (1998) “Design provisions for earthquake resistance of structures”, ENV 1998, 1-1/3, *CEN*, Brussels.

FIB bulletin 25: Displacement-based seismic design of reinforced concrete buildings (2003), State-of-art report prepared by Task Group 7.2 “Displacement-based design and assessment”, *Federation Internationale du Beton*, ISBN 2-88394-065-7, Printed by Sprint-Digital-Druck Stuttgart.

Gulkan P., Sozen M. (1974) “Inelastic response of reinforced concrete structures to earthquakes motions”, *ACI Journal*, 71: 604-610.

Hadjian A. H. (1982) “A re-evaluation of equivalent linear models for simple yielding systems”, *Earthquake Engineering and Structural Dynamics*, 10: 759-767.

Hill K. E. (1968) “Dynamic properties of ring springs for use as seismic energy dissipaters”, *Proceedings of NZSEE Technical Conference*, Norway.

Iwan W. D. (1980) “Estimating inelastic response spectra from elastic response spectra”, *Earthquake Engineering and Structural Dynamics*, 8: 375-388.

Iwan W. D., Gates N. C. (1979) “The effective period and damping of a class of hysteretic structures”, *Earthquake Engineering and Structural Dynamics*, 7: 199-211.

Iwan W. D., Gates N. C. (1979) “Estimating earthquake response of simple hysteretic structures”, *Journal of the Engineering Mechanics Division*, Vol. 105, No. EM3: 391-405.

Jacobsen L. S. (1930) “Steady forced vibrations as influenced by damping”, *ASME Transactions*, 52(1): 169-181.

Jacobsen L. S. (1960) “Damping in composite structures”, *Proceedings of Second World Conference on Earthquake Engineering,* Tokyo and Kyoto, Japan, Vol. 2: 1029-1044.

Jennings P. (1968) “Equivalent damping for yielding structures”, *Journal of Engineering Mechanics Division ASCE*, 94: 103-116.

Jennings P. C., Housner G. W., Tsai N. C. (1968) “Simulated Earthquake motions”, *Earthquake Engineering Research Laboratory*, California Institute of Technology, April.

Kowalsky M. J. (1994) “Displacement-based design methodology for seismic design applied to RC bridge columns”, Master’s Thesis, *University of California*, San Diego.

Kowalsky M. J., Priestley M. J. N., MacRae G. A. (1994) “Displacement-based design: A methodology for seismic design applied to single degree of freedom reinforced concrete structures”, *University of California*, San Diego, Structural Systems Research project, Report No. SSRP-94/16.

Kowalski M., Dwairi H. (2004) “Examination of the equivalent viscous damping approach”, *International Workshop on Performance-Based Seismic Design Concepts and Implementation*, Bled, Slovenia, 28 June – 1 July.

Mahin S. A., Lin J. (1983) “Construction of inelastic response spectra for single degree of freedom systems”, Report No. UCB/EER-83/17, EERC, *University of California at Berkley*.

Millard A. (1993) CASTEM 2000, Guide d’utilisation, Rapport CEA 93/007, Saclay, France.

Miranda E., Ruiz-Garcia R. (2002) “Evaluation of approximate methods to estimate maximum inelastic displacement demands”, *Earthquake Engineering and Structural Dynamics*, 31: 539-560.

Priestley M. J. (2003) “Myths and fallacies in earthquake engineering”, revisited, *The Mallet Milne Lectures*, IUSS Press, Pavia, Italy.

Rosenblueth E., Herrera I. (1964) “On a kind of hysteretic damping”, *Journal of the Engineering Mechanics Division*, ASCE, Vol. 90, No. EM4, pp. 37-38

Shibata A., Sozen M. (1976) “Substitute structure method for seismic design in reinforced concrete”, *Journal of Structural Division*, ASCE, Vol. 102, No. 1: 1-18.

Takeda T., Sozen M., Nielsen N. (1970) “Reinforced concrete response to simulated earthquakes”, *ASCE Proceedings*, Vol. 96, ST12, pp. 2557-2573.

European Commission

**EUR 23365 EN – Joint Research Centre – Institute for the Protection and Security of the Citizen**
Title: Equivalent period and damping for EC8 spectral response of SDOF ring-spring hysteretic systems
Author(s): Raul ZAHARIA and Fabio TAUCER
Luxembourg: Office for Official Publications of the European Communities
2008 – 66 pp. – 21 x 29.7 cm
EUR – Scientific and Technical Research series – ISSN 1018-5593

**Abstract**
The following report presents a procedure to determine the equivalent properties of a viscoelastic linear model capable of approximating the maximum earthquake response of a SDOF ring-spring hysteretic system, representative of the cyclic behaviour of lightly reinforced concrete bridge piers, for a series of synthetic ground motions compatible with Type 1 and Type 2 Eurocode 8 spectra. The results show that the displacements obtained from the equivalent model approximate well the results obtained from the nonlinear model, and that the coefficients of the expressions for determining the equivalent properties depend on the family of earthquakes considered in the analysis. Expressions for determining the secant stiffness and equivalent damping corresponding to the energy dissipated by harmonic cycles at maximum displacement are derived for the ring-spring model and a relationship for computing a reduction factor of the maximum ductility is proposed such that the equivalent properties computed from these expressions approximate those obtained from the error minimization process. Recommendations to improve the error minimization process and the derivation of equivalent properties are proposed at the end of the report.

The mission of the JRC is to provide customer-driven scientific and technical support for the conception, development, implementation and monitoring of EU policies. As a service of the European Commission, the JRC functions as a reference centre of science and technology for the Union. Close to the policy-making process, it serves the common interest of the Member States, while being independent of special interests, whether private or national.